**Climate
of the Past**
Open Access
Discussions

Benthic foraminifera at the Paleocene/Eocene thermal maximum in the western Tethys (Forada section): variability in climate and productivity

L. Giusberti[1], F. Boscolo Galazzo[1], and E. Thomas[2,3]

[1]Department of Geosciences, University of Padova, Via Gradenigo 6, 35131 Padova, Italy
[2]Department of Geology and Geophysics, Yale University, 210 Whitney Avenue, New Haven 06511, USA
[3]Department of Earth and Environmental Sciences, Earth and Environmental Sciences, Wesleyan University, 265 Church Street, Middletown, 06459, USA

Correspondence to: L. Giusberti (luca.giusberti@unipd.it)

Discussion Paper | Discussion Paper | Discussion Paper | Discussion Paper

CPD

11, 4205–4272, 2015

Benthic foraminifera at the Paleocene/Eocene thermal maximum

L. Giusberti et al.

Title Page

Abstract	Introduction
Conclusions	References
Tables	Figures

|◄ | ►|
| ◄ | ► |

Back | Close

Full Screen / Esc

Printer-friendly Version

Interactive Discussion

Abstract

The Forada section (northeastern Italy) provides a continuous, expanded deep-sea record of the Paleocene/Eocene thermal maximum (PETM) in the central-western Tethys. We combine a new, high resolution, benthic foraminiferal assemblage record with published calcareous plankton, mineralogical and biomarker data to document climatic and environmental changes across the PETM, highlighting the benthic foraminiferal extinction event (BEE). The onset of the PETM, occurring ~ 30 kyr after a precursor event, is marked by a thin, black, barren clay layer, possibly representing a brief pulse of anoxia and carbonate dissolution. The BEE occurred within the 10 cm interval including this layer. During the first 3.5 kyr of the PETM several agglutinated recolonizing taxa show rapid species turnover, indicating a highly unstable, CaCO$_3$-corrosive environment. Calcareous taxa reappeared after this interval, and the next ~ 9 kyr were characterized by rapid alternation of peaks in abundance of various calcareous and agglutinant recolonizers. These observations suggest that synergistic stressors including deep water CaCO$_3$-corrosiveness, low oxygenation, and high environmental instability caused the extinction. Combined faunal and biomarker data (BIT index, higher plant *n*-alkane average chain length) and the high abundance of the mineral chlorite suggest that erosion and weathering increased strongly at the onset of the PETM, due to an overall wet climate with invigorated hydrological cycle, which led to storm flood-events carrying massive sediment discharge into the Belluno Basin. This interval was followed by the core of the PETM, characterized by four precessionally paced cycles in CaCO$_3$%, hematite%, δ^{13}C, abundant occurrence of opportunistic benthic foraminiferal taxa, as well as calcareous nannofossil and planktonic foraminiferal taxa typical of high productivity environments, radiolarians, and lower δD$_{n\text{-alkanes}}$. We interpret these cycles as reflecting alternation between an overall arid climate, characterized by strong winds and intense upwelling, with an overall humid climate, with abundant rains and high sediment delivery (including refractory organic carbon) from land. Precessionally paced marl-limestone couplets occur throughout the

Benthic foraminifera at the Paleocene/Eocene thermal maximum

L. Giusberti et al.

Printer-friendly Version

Interactive Discussion

recovery interval of the CIE and up to ten meters above it, suggesting that these wet-dry cycles persisted, though at declining intensity, after the peak PETM. Enhanced climate extremes at mid-latitudes might have been a direct response to the massive CO_2 input in the ocean atmosphere system at the Paleocene–Eocene transition, and may have had a primary role in restoring the Earth system to steady state.

1 Introduction

The Paleocene–Eocene Thermal Maximum (PETM) has over the last twenty four years attracted intensive study by the scientific community, as one of the most dramatic and rapid climatic disruptions of the Cenozoic (e.g., Kennett and Stott, 1991; Zachos et al., 2001; Sluijs et al., 2007a; McInerney and Wing, 2011; Littler et al., 2014). During the PETM (~ 55.6 Ma), the Earth's surface temperature increased by $\sim 5\,°C$ in a few thousand years (McInerney and Wing, 2011; Dunkley-Jones et al., 2013; Zeebe et al., 2014; Bowen et al., 2015), and remained high for 100 to 170–200 kyr (e.g., Roehl et al., 2007; Giusberti et al., 2007; Murphy et al., 2010). The PETM is recognized in terrestrial and marine settings by a negative carbon isotope excursion (CIE; e.g., Kennett and Stott, 1991; Bowen et al., 2004), with variable magnitude ranging from ~ 2–4.5‰ in marine carbonates (e.g., Thomas and Shackleton, 1996; Bains et al., 1999; Thomas et al., 2002; Zachos et al., 2006; Handley et al., 2008; McCarren et al., 2008) to 4–7‰ in marine and terrestrial organic carbon and leaf waxes (e.g., Kaiho et al., 1996; Bowen et al., 2004, 2015; Pagani et al., 2006a; Smith et al., 2007; Handley et al., 2008; McCarren et al., 2008). This CIE is attributed to a massive, rapid input of isotopically light carbon into the ocean–atmosphere system, which destabilized the global carbon cycle and led to rapid and extreme global warming (e.g., Dickens et al., 1995; Thomas and Shackleton, 1996; Pagani et al., 2006b; Panchuk et al., 2008; Dickens, 2011; DeConto et al., 2012). Both the source(s) of the carbon and the triggering mechanism(s) of the emissions are still strongly debated (e.g., Meissner et al., 2014), in part because the pattern and size of the CIE does not necessarily simply reflect the size and isotopic sig-

nature of the carbon input, but is affected by sedimentary processes (Kirtland Turner and Ridgwell, 2013)

Despite these debates, the onset of the CIE is an outstanding global correlation tool (McInerney and Wing, 2011; Stassen et al., 2012b), formally used to define the base of the Eocene (Aubry et al., 2007). The carbon cycle perturbation of the PETM led to acidification of surface ocean waters (Penman et al., 2014) and profound shallowing of the calcite compensation depth (CCD; Zachos et al., 2005; Kelly et al., 2010; Hönisch et al., 2012). Widespread carbonate dissolution coincided with the base of the CIE (e.g., Thomas and Shackleton, 1996; Thomas, 1998; Hancock and Dickens, 2005; McCarren et al., 2008). The profound paleoceanographic changes affected primary and export productivity (e.g., Thomas, 2007; Winguth et al., 2012; Ma et al., 2014), which in general increased in marginal basins and along continental margins, but decreased in open oceans (e.g., Gibbs et al., 2006; Stoll et al., 2007; Speijer et al., 2012). The higher ocean temperatures may have led to increased remineralization of organic matter in the oceans due to increased metabolic rates (John et al., 2013, 2014; Boscolo Galazzo et al., 2014). The combination of increased remineralization, higher temperatures and increased ocean stratification led to a decrease of oxygen levels in bottom waters regionally, especially along continental margins (including the Arctic Ocean) and in the Atlantic Ocean (e.g, Thomas, 2007; Chun et al., 2010; Speijer et al., 2012; Winguth et al., 2012; Wieczorek et al., 2013; Dickson et al., 2014; Paelike et al., 2014; Post et al., 2015), while Oxygen Minimum Zones in open oceans expanded globally (Zhou et al., 2014), including at Forada (Luciani et al., 2007).

The increased primary productivity in marginal basins has been linked to increased influx of nutrients from the continents caused by increased erosion and weathering due to intensification of the hydrological cycle, because precipitation is correlated to globally-averaged surface temperatures (e.g., Pierrehumbert, 2002). A widespread increase in kaolinite in PETM sediments has been related to the global increase in precipitation and intensity of chemical weathering (e.g., Robert and Chamley, 1991; Robert and Kennett, 1994; Kaiho et al., 1996; Gibson et al., 2000; Fig. 1 and Table S1 in the

Supplement), as also suggested by Os-isotope evidence (Ravizza et al., 2001; Wieczorek et al., 2013). However, reconstruction of hydrological changes from clay mineral assemblages is complex, and additional evidence is needed (Thiry, 2000; Schmitz and Pujalte, 2003, 2007; Egger et al., 2003, 2005; Handley et al., 2012).

At the onset of the PETM, middle to subtropical latitudes may have been characterized by intense, monsoonal-type rainfall, followed – during the core of the PETM – by a succession of wet and arid phases, possibly precessionally paced, (e.g., Krauss and Rigging, 2007; Egger et al., 2009; Stassen et al., 2012a, b, 2015; Fig. 1 and Table S1). Increased storminess and frequency of flooding events at the onset of the PETM was documented in the Tremp–Graus Basin (Pyrenees), in a zone with a generally dry climate (the subtropical net evaporation zone, 15–35° N). The onset of the PETM may have coincided with increased seasonal humidity gradients, triggering intense flash floods in that region (Schmitz and Pujalte, 2007). Episodic fire and post-fire runoff events occurred across the PETM in the London basin (Collison et al., 2007; Foreman et al., 2014; Table S1).

In the northern rain belt and into the Arctic basin (> 50° N), humid conditions may have been more persistent, with increased rates of precipitation, and on average moister conditions during the PETM (Pagani et al., 2006b, Sluijs et al., 2006; Harding et al., 2011; Dypvik et al., 2011; Kender et al., 2012; Wieczorek et al., 2013; Table S1). The net result of increased weather extremes during peak-PETM might have been to decrease rainout at subtropical to mid latitudes, and increase moisture transport toward the high latitudes (Pagani et al., 2006b). Few tropical records exist, so that precipitation changes are less clear. Rainfall in coastal Tanzania may have decreased during the early PETM, but combined with violent precipitation events and flooding (Handley et al., 2008, 2012; Aze et al., 2014; Table S1). In Central America, conditions may have shifted to more continuously humid (Jaramillo et al., 2010).

These severe climatic perturbations profoundly affected terrestrial and marine ecosystems, triggering faunal and floral radiations and migrations (e.g., Kelly et al., 1996; Bralower, 2002; Gingerich, 2003; Wing et al., 2005; Sluijs et al., 2007; Jaramillo

Title Page

Abstract | Introduction

Conclusions | References

Tables | Figures

|◄ | ►|

◄ | ►

Back | Close

Full Screen / Esc

Printer-friendly Version

Interactive Discussion

et al., 2010; McInerney and Wing, 2011). Deep-sea benthic foraminifera experienced the most severe extinction of the Cenozoic, the benthic foraminiferal extinction event (BEE) (Thomas, 1989, 1990, 1998; Kennett and Stott, 1991; Thomas and Shackleton, 1996; Alegret et al., 2009a, b; 2010). The BEE was rapid (< 10 kyr; Thomas, 1989, 2003, 2007), and wiped out the Cretaceous bathyal and abyssal "Velasco-type fauna" (Berggren and Aubert, 1975; Tjalsma and Lohmann, 1983; Thomas, 1998, 2007), marking a significant step towards the establishment of modern benthic foraminiferal fauna (Thomas, 2007). The extinction was far less severe in shelf environments (Gibson et al., 1993; Speijer, 2012; Stassen et al., 2015).

The cause of this global extinction remains under debate, because neither anoxia nor higher or lower productivity, nor carbonate dissolution occurred globally at bathyal to abyssal depths in the deep sea, the largest habitat on Earth (e.g., Thomas, 2003, 2007; Alegret et al., 2010), and benthic foraminifera are highly efficient dispersers (Alve and Goldstein, 2003). The link between the environmental changes during the PETM and the benthic foraminiferal extincton event thus remains poorly understood. A common obstacle to performing detailed high-resolution studies of the PETM in deep-sea sediments is the fact that many records are condensed or discontinuous, especially across the few thousand years (Zeebe et al., 2014) of the onset of the carbon isotope excursion.

The Forada section (northeastern Italy) represents an outstanding exception in that it contains an expanded deep-sea record of the PETM, which has been extensively studied because of its continuity and cyclostratigraphy (Agnini et al., 2007; Giusberti et al., 2007; Luciani et al., 2007; Tipple et al., 2011; Dallanave et al., 2012). Carbonate dissolution is less severe at Forada than in many other sections, with calcareous benthic foraminifera present for most of the interval characterized by the CIE (> 4 m; Giusberti et al., 2007). Given the limited number globally of complete and expanded deep-sea PETM sections, the Forada section represents an invaluable opportunity to investigate the environmental impacts of the PETM and repercussions on deep-sea fauna.

Title Page

Abstract | Introduction

Conclusions | References

Tables | Figures

◀◀ | ▶▶

◀ | ▶

Back | Close

Full Screen / Esc

Printer-friendly Version

Interactive Discussion

We provide a high-resolution benthic foraminiferal record for the Forada section, in order to reconstruct the progression (tempo and mode) of environmental and biotic changes during the PETM. These data allow us to reconstruct the environmental disruption and the benthic foraminiferal response to PETM warming in detail, and document the community recovery. Benthic foraminiferal data are integrated with sedimentological and geochemical data (Giusberti et al., 2007; Tipple et al., 2011), and data on calcareous plankton communities (Agnini et al., 2007; Luciani et al., 2007), providing perhaps the most complete reconstruction across the PETM in Europe todate.

We pay homage to research by Italian researchers (Di Napoli Alliata et al., 1970; Braga et al., 1975), who first described the benthic foraminiferal turnover across the Paleocene–Eocene transition in Italy.

2   Materials and methods

2.1   The Forada section

The Forada section (46.036083° N, 12.063975° E) is exposed along the Forada creek, ∼ 2 km east of the village of Lentiai (Fig. 2) in the Venetian Pre-Alps (NE Italy). It consists of ca. 62 m of Scaglia Rossa, pink-reddish limestones and marly limestones, locally rhythmically bedded, and encompassing the Upper Cretaceous through the lower Eocene (Fornaciari et al., 2007; Giusberti et al., 2007). The upper Paleocene–lower Eocene succession is interrupted by the clay marl unit (CMU; Giusberti et al., 2007), which marks the PETM and correlates with clay-rich units on other continental margins (e.g., Schmitz et al., 2001; Crouch et al., 2003; John et al., 2008; Nicolo et al., 2010). The investigated interval has been subdivided into four sub-intervals based on the δ^{13}C record in bulk rock (Giusberti et al., 2007). From bottom to top, these are the pre-CIE, the main CIE, the CIE recovery and post-CIE (Fig. 3).

The main CIE (Giusberti et al., 2007; Fig. 3) occurs in the > 3 m-thick CMU, within which are recorded the short-lived occurrences of the calcareous plankton "excursion

Benthic foraminifera at the Paleocene/Eocene thermal maximum

L. Giusberti et al.

Title Page

Abstract | Introduction

Conclusions | References

Tables | Figures

|◄ | ►|

◄ | ►

Back | Close

Full Screen / Esc

Printer-friendly Version

Interactive Discussion

taxa" (Kelly et al., 1996, 1998) and the BEE (Agnini et al., 2007; Giusberti et al., 2007; Luciani et al., 2007). Sedimentation rates in the CMU were five times higher than in the upper Paleocene, indicating increased continental weathering and run-off, which led to increased sediment influx in the Belluno Basin (Giusberti et al., 2007).

2.2 Benthic foraminifera

Benthic foraminiferal assemblages were studied in 54 samples across an ∼ 11 m-thick interval straddling the PETM (−467 to +591.5 cm; Fig. 3), which reflects ∼ 800 kyr (Giusberti et al., 2007). Sample spacing was determined based on biostratigraphic and cyclostratigraphic data (Agnini et al., 2007; Giusberti et al., 2007; Luciani et al., 2007). A sampling interval of 3–5 cm was used across the onset of the CIE (−42.5 to +50 cm interval), a 25 cm sample interval over the main CIE (from +75 to 335 cm). Below −42.5 and above 335 cm we adopted a spacing between 20 and 50 cm. Foraminifera were extracted from the indurated marls and limestones using the "cold acetolyse" technique of Lirer (2000), following Luciani et al. (2007). Soft marly samples (mostly from the CMU interval) were disaggregated using a 10–30 % solution of hydrogen peroxide.

The quantitative study was based on representative splits (using a micro-splitter Jones, Geneq Inc.) of approximately 200–400 individuals $> 63 \, \mu m$ and $< 500 \, \mu m$ (Table S2). The use of the small-size fraction is time-consuming and presents difficulties in taxonomic determination, but we preferred to avoid the loss of small taxa, which are important for paleoecological investigations (e.g., Thomas, 1985; Boscolo Galazzo et al., 2013, 2015), especially directly after the BEE when small species are dominant (Thomas, 1998; Foster et al., 2013). Between 0 and −222 cm (uppermost Paleocene), the fraction $\geq 125 \, \mu m$ of at least 1/4 of the residue was carefully scanned for large specimens of the extinction taxa, here labeled "cosmopolitan extinction taxa" (CET) (see Thomas, 1998, 2003). These CET records have been treated qualitatively (Fig. S1). The extinction taxa include: *Anomalinoides rubiginosus*, *Angulogavelinella avnimelechi*, *Aragonia velascoensis*, *Bolivinoides delicatulus*, *Cibicidoides dayi*, *C. hyphalus*, *C. velascoensis*, *Clavulina amorpha*, *Clavulinoides trilatera*, *Clavulinoides*

globulifera, *Coryphostoma midwayensis*, *Dorothia beloides*, *D. bulletta*, *D. pupa*, *D. retusa*, *Neoeponides megastoma*, *Gavelinella beccariiformis*, *Gyroidinoides globosus*, *G. quadratus*, *Marsonella indentata*, *Neoflabellina jarvisi, N. semireticulata*, *Nuttallinella florealis*, *Osangularia velascoensis*, *Paralabamina hillebrandti*, *P. coryelli*, *Remesella varians* (e.g., Beckmann, 1960; Von Hillebrandt, 1962; Tjalsma and Lohmann, 1983; Speijer et al., 1996; Thomas, 1998), each of which is present at Forada.

We identified most common taxa at the species level (Table S3). Taxa with high morphological variability and/or variable preservation were identified at generic or higher taxonomic level. Specimens of the most representative taxa were imaged using the SEM at the C.U.G.A.S. (Centro Universitario Grandi Apparecchiature Scientifiche) of Padova University (Plates I–IV). Relative abundances of the taxa and taxon-groups, along with faunal indices such as the calcareous-agglutinated ratio, the infaunal-epifaunal ratio, and bi-triserial percentage were calculated (Figs. 3, 5 and 6 and Fig. S2). The absolute abundance (N g^{-1}: number of benthic foraminifera per gram-bulk dried sediment) was calculated for both the $\geq$ 63 and $\geq$ 500 μm fractions. Faunal diversity indexes (Species diversity and Fisher-α; Fig. 3) were calculated using the PAST package (Hammer et al., 2001). We assigned species to epifaunal and infaunal groups by comparing their test morphology to the morphogroups in Corliss (1985), Jones and Charnock (1985), Corliss and Chen (1988) and Kaminski and Gradstein, (2005), Hayward et al. (2012), and Mancin et al. (2013). Segments belonging to tubular/branched agglutinated forms (e.g., *Rhizammina, Rhabdammina, Bathysiphon*) were counted, but excluded from calculations because there is no reliable method to convert the abundance of multiple fragments into that of single individuals (Ernst et al., 2006). Following Hancock and Dickens (2005), the fragmentation index (F Index) of planktic foraminifera (Luciani et al., 2007) is used as a proxy for dissolution (Figs. 3 and 4).

2.2.1 Paleocene–Eocene benthic foraminiferal ecology

We first summarize and discuss the ecology of benthic foraminiferal taxa that played a key-role during the PETM. We allocated the taxa to the categories recolonizers (R1,

R2) and opportunistics (O1, O2), based on their abundance pattern in the studied and other PETM sections. With the term "recolonizers" we indicate highly stress-tolerant, opportunistic taxa that repopulated the sea floor in the earliest phases of benthic foraminiferal recovery. We prefer to avoid the term "disaster taxa" because at Forada the recolonizers do not strictly follow the pattern of disaster taxa (Kauffman and Harries, 1996; Harries et al., 1996), in that most of the recolonizers at Forada persist or peak again in the later phase of recovery. The term "opportunistic", as adopted here, follows the definition in Kauffman and Harries (1996) and Harries et al. (1996).

(R1) Agglutinant recolonizers: *Haplophragmoides* spp., *Glomospira* spp., *Eobigenerina variabilis,* saccamminids, *Ammobaculites agglutinans* and karrerulinids.

Most of these are typical for post-extinction assemblages in Tethyan PETM records (e.g., Ortiz et al., 1995; Egger et al., 2005; Ernst et al., 2006; Alegret et al., 2009a; Giusberti et al., 2009; Arreguin-Rodriguez et al., 2013, 2014), except *E. variabilis* and *A. agglutinans,* which have not been described from other Tethyan sections. *Eobigenerina variabilis*, *Ammobaculites agglutinans*, *Haplophragmoides* spp., *Glomospira* spp. and saccamminids are known as "pioneer forms", capable of rapid recolonization of sediments after major environmental disruptions due to their high dispersal capability (e.g., Kuhnt and Kaminski, 1993; Kuhnt, 1992; Galeotti et al., 2002; Friedrich, 2009; Ly and Kuhnt, 1994; Kaminski et al., 1996; Cetean et al., 2008a, b; Waśkowska A., 2011).

Eobigenerina, a recently erected genus in the Textulariopsidae, includes non-calcareous species previously assigned to *Bigenerina* (Cetean et al., 2011). Similar taxa with a biserial to uniserial chamber arrangement (e.g. *Rashnovammina*, *Bicazammina* etc.) are grouped as "pseudobolivinids" (Fig. 6). Such forms occur in Paleocene–Eocene Scaglia sediments of the Umbria–Marche basin (Contessa section), and have been commonly referred to as *Pseudobolivina* (e.g., Galeotti et al., 2004; Giusberti et al., 2009).

Title Page

Abstract | Introduction

Conclusions | References

Tables | Figures

◀ | ▶|

◀ | ▶

Back | Close

Full Screen / Esc

Printer-friendly Version

Interactive Discussion

Ammobaculites agglutinans and *Saccammina* are common in modern high productivity areas, or regions with abundant but periodically supplied organic matter (Gooday et al., 2001, 2008; Gooday, 2003). Modern representatives of *Karrerulina* (e.g. *K. apicularis = K. conversa*) are part of an oligotrophic biofacies on abyssal plains with well-oxygenated bottom and interstitial waters (Kuhnt et al., 2000; Kaminski and Gradstein, 2005). However, the *Karrerulina* test morphology, combined with its abundant occurrence in the aftermath of the PETM at Forada, suggests that this genus may also act opportunistically. It has been recognized in the lowermost Eocene in drill sites in the Iberia abyssal plan (Kuhnt and Collins, 1996).

Glomospira species are very abundant in the lowermost Eocene at several deep water locations, including in the Tethys and North Atlantic (the "*Glomospira* acme", e.g., Kuhnt and Collins, 1996; Galeotti et al., 2004; Kaminski and Gradstein, 2005; Arreguin-Rodriguez et al., 2013), and have been interpreted as oligotrophic indicators (e.g., Galeotti et al., 2004; Kaminski and Gradstein, 2005), though they could be indicative of an abundant supply of terrigenous, refractory organic matter, independent from local primary productivity (Arreguin-Rodriguez et al., 2013).

(R2) Hyaline recolonizers: *Globocassidulina subglobosa*, *Osangularia* spp., *Oridorsalis umbonatus* and *Tappanina selmensis*.

These species increase in abundance in the basal PETM, just above the agglutinant-dominated interval in the Spanish Alamedilla and Caravaca sections (Ortiz, 1995; Alegret et al., 2009a, 2011) as well as the Italian Contessa Road section (Giuberti et al., 2009; Fig. S3). *G. subglobosa* is a cosmopolitan, highly adaptable, long-ranging opportunistic species. Modern representatives of this species have been described from a wide variety of environmental settings (Singh and Gupta, 2004). Several authors suggested that it feeds on phytodetritus (e.g. Gooday, 1993, 1994; Jorissen et al., 2007) and reflects pulsed food supply to the sea floor (Nomura, 1995; Gupta and Thomas, 2003; Suhr et al., 2003; Gooday et al., 2008; Takata et al., 2010) in oxygenated deep-water settings (Mohan et al., 2011). It is, for instance, an abundant species at high

Benthic foraminifera at the Paleocene/Eocene thermal maximum

L. Giusberti et al.

Full Screen / Esc

Printer-friendly Version

Interactive Discussion

southern latitudes where seasonality is extreme (e.g., Ishman and Domack, 1994; Murray and Pudsey, 2004). However, Panieri and Sen Gupta (2007) found *G. subglobosa* on the Blake Ridge hydrate mound, within sediments rich in organic matter, and Sgarrella et al. (1997) interpreted high abundances of *G. subglobosa* in the basal Pliocene
5 Trubi formation (Italy) as indicative of increased productivity. At many sites, *G. subglobosa* first appears after the BEE (e.g, Maud Rise, Thomas, 1990, 1998; Thomas and Shackleton, 1996; Pacific Ocean, Thomas, 1998; Takeda and Kaiho, 2007); but at other locations it is present from the uppermost Paleocene on (e.g., Walvis Ridge, Thomas and Shackleton, 1996). Takeda and Kaiho (2007) consider it an opportunistic species,
10 blooming after the BEE.

During the Cretaceous Oceanic Anoxic Events (OAEs), *Osangularia* spp. opportunistically repopulated the sea floor during short-term re-oxygenation phases (e.g., Holbourn et al., 2001; Friedrich et al., 2005; Friedrich, 2009). According to Holbourn and Kuhnt (2001), *Osangularia* behaved as opportunistic phytodetritus feeders dur-
15 ing OAE1b, thriving on an enhanced carbon flux to the sea floor and tolerating some degree of oxygen depletion.

Oridorsalis umbonatus is a very long-ranging, extant taxon (since the Coniacian, Kaiho, 1998; present in the Turonian, Wendler et al., 2013) with an opportunistic lifestyle, which thrives under a large variety of environmental conditions: it has been re-
20 ported both in oligotrophic and eutrophic environments (e.g. Schmiedl, 1995; Schmiedl and Mackensen, 1997; Gupta and Thomas, 1999; Gupta et al., 2008). Gooday (1993, 1994) suggested that it may feed on phytodetritus, but its stable isotope signature indicates it is a shallow infaunal dweller (Thomas and Shackleton, 1996; Katz et al., 2003). It has very small tests but with increased calcification just above the base of the PETM
25 at Walvis Ridge (SE Atlantic) Site 1263, where it dominates the assemblage (Foster et al., 2013).

Tappanina selmensis may be another indicator of high-productivity (Kuhnt, 1996 and Kuhnt and Kaminski, 1996), and is a stress-tolerant and opportunistic species (e.g., Thomas, 1989, 1990, 1998; Thomas and Shackleton, 1996; Steineck and Thomas,

1996; Giusberti et al., 2009; Alegret et al., 2009a; D'haenens et al., 2012), possibly thriving in continuously stressed, possibly dysoxic sea bottom conditions (Stassen et al., 2012b). *Tappanina selmensis* was an upper bathyal to outer shelf species in the Campanian through Paleocene (van Morkhoven et al., 1986; Frenzel, 2000; Stassen et al., 2012a, 2015), becoming common in the deep-sea only just before and especially after the BEE (Tjalsma and Lohmann, 1983; Boersma, 1984; Thomas, 1990, 1998).

(O1) Agglutinant opportunists: *Spiroplectammina navarroana*

Spiroplectammina navarroana was probably an opportunistic taxon, known from a few bathyal sections as minor component of PETM post-extinction faunas (e.g., Ortiz, 1995; Alegret et al., 2009b). At some locations, it is common just after the Cretaceous/Paleogene boundary (Alegret et al., 2003).

(O2) Hyaline opportunists with tapered elongate tests: *Siphogenerinoides brevispinosa*, stilostomellids and pleurostomellids.

Siphogenerinoides brevispinosa flourished at many open ocean sites in the aftermath of the peak CIE (Thomas, 2003, 2007; Giusberti et al., 2009), and is considered by Thomas (2003) a bloom species, i.e., an opportunist capable to rapidly colonize the sediment when productivity increases during environmental instability. At some locations (e.g., Maud Rise in the Southern Oceans) it bloomed during the PETM and other hyperthermals (Thomas, 1998; Thomas and Shackleton, 1996), at others (equatorial Pacific Site 865) it had its highest occurrence in the lowermost part of the PETM (Thomas, 1998).

Stilostomellids and pleurostomellids were widely distributed in oligotrophic and eutrophic regions with sustained or highly seasonal phytoplankton productivity (Hayward et al., 2010b, 2012) and tolerated warm, locally oxygen-depleted, carbonate-corrosive bottom waters, as demonstrated by their survival across the PETM (Hayward et al., 2010a, 2012). Across Cretaceous OAEs, pleurostomellids were found within black-

shales (e.g., Coccioni and Galeotti, 1993; Holbourn and Kuhnt, 2001; Friedrich et al., 2005; Friedrich, 2009), indicating they may have been adapted to low-oxygen conditions, or may have been able to rapidly recolonize the sea-floor during brief intervals of reoxygenation. The Families Stilostomellidae and Pleurostomellidae dominated deep-sea faunas in the middle–late Eocene with their maximum abundance reaching up to 50–75 % at bathyal–upper abyssal depths, declined in abundance during the cooling of the earliest Oligocene and middle Miocene, to become extinct in the middle Pleistocene (e.g., Gooday and Thomas, 1996; Thomas, 2007; Hayward et al., 2012). Their association with infaunal taxa and stable isotope composition indicates they were infaunal (Mancin et al., 2014).

Caution is needed in applying taxonomic uniformitarianism due to our limited knowledge of the biology and ecology of the highly diverse living species. Even for many living species, the relation between test morphology and microhabitat has not been directly observed, but is extrapolated from data on other taxa (e.g., Jorissen, 1999). The assignment of modern foraminifera to microhabitats based on their morphology may be accurate only about 75 % (Buzas et al., 1993): comparisons between past and recent environments thus need careful evaluation, and cross correlation between benthic foraminiferal and other proxy data.

2.3 Age model

The age model used for calculating the longevity of benthic foraminiferal assemblages (see below) follows Luciani et al. (2007), with the lower Eocene chronology based on the cyclostratigraphic age model of Giusberti et al. (2007; Fig. 4). The duration of each precessional cycle has been assumed to be 21 kyr. Sedimentological and geochemical parameters oscillate cyclically within the main CIE, in at least five complete precessional cycles (Figs. 3 and 4). The CIE recovery interval is composed of six distinct, precessional marly-limestone couplets cycles (Fig. 3). The recognition of eleven cycles in the combined CIE and recovery interval implies an estimate of the total duration of the CIE of ca. 230 kyr (Fig. 4). Giusberti et al. (2007) and Roehl et al. (2007) disagree

Benthic foraminifera at the Paleocene/Eocene thermal maximum

L. Giusberti et al.

Title Page

Abstract	Introduction
Conclusions	References
Tables	Figures

◄ | ►

◄ | ►

Back | Close

Full Screen / Esc

Printer-friendly Version

Interactive Discussion

on the duration of the main CIE and recovery interval (179 ± 17 and 231 ± 22 kyr, respectively). The main difference between these two chronologies is the assignment of different numbers of precessional cycles within the main body and recovery interval (Tipple et al., 2011). A [3]He-based chronology for Site 1266 (Walvis Ridge) suggests a total PETM duration of $234 +48/-34$ kyr (Murphy et al., 2010), in line with the age model of Giusberti et al. (2007).

In the Paleocene, lithological cycles have not been firmly identified, and sedimentation rates are interpolated between the base of the PETM at ± 0 cm and the lowest occurrence of the calcareous nannofossil *Discoaster multiradiatus* at ca. -12.5 m (Giusberti et al., 2007), using a duration of the time between these events of 1.238 Myr (Westerhold et al., 2007). In this age model, the investigated portion of Forada section spans ca. 800 kyr.

3 Results

Benthic foraminiferal assemblages are generally dominated by calcareous hyaline taxa (85–90 %; Fig. 3), but agglutinated taxa significantly increase in abundance within the CMU (25–90 %; Fig. 3). Infaunal taxa strongly dominate the assemblage throughout the studied interval (~ 80 %). Faunal diversity is fairly high, particularly in the upper Paleocene (Fig. 3), and preservation is generally moderate, though poor within the lowermost centimeters of the Eocene.

Composition and abundance of the assemblages change prominently across the ca. 11 m-thick interval investigated (Figs. 3, 5 and 6), coeval with the geochemical signature of the PETM, thus broadly coincident with the main lithological changes. We recognized six successive benthic foraminiferal assemblages (labeled A to F; Figs. 3 and 5–8), mainly based on changes in abundance of the taxa listed above. Assemblages A and B are characteristic of the dominantly reddish calcareous marls of the uppermost Paleocene, separated by the thin, barren clay layer from Assemblages C, D and E, which occur in the first half of the main excursion of the CIE (lowermost Eocene),

Benthic foraminifera at the Paleocene/Eocene thermal maximum

L. Giusberti et al.

within the CMU (green and reddish clays, marly clays and marls). Assemblage F characterizes the marls of the upper half of the CMU, as well as the CIE recovery interval and the overlying post-excursion interval of reddish limestone–marl couplets (Giusberti et al., 2007).

3.1 Assemblage A: the upper Paleocene fauna

Assemblage A (−467.5 to −37.5 cm, estimated duration > 430 kyr) has a high diversity, with abundant infaunal taxa (ca. 70–80 %; Fig. 3). Small bolivinids (< 125 µm) of the *Bolivinoides crenulata* group (Plate 3, Figs. 7–9), and smooth-walled *Bolivina* spp. together comprise 50–60 % of the > 63 µm fauna (Fig. 5), with *Siphogenerinoides brevispinosa* and *Bulimina* spp. less common (∼ 10 %; Figs. 5 and 6). Epifaunal morphotypes are mainly represented by small cibicidids (10 %), *Anomalinoides* spp. (5 %) and *Cibicidoides* spp. (usually < 5 %). Rare taxa include reussellids, angulogerinids, nodosariids, dentalinids, gyroidinids, valvalabaminids and unilocular hyaline taxa. Agglutinated taxa are mainly represented by *Spiroplectammina spectabilis*, *Trochamminoides* spp., *Paratrochamminoides* spp., *Reophax* spp. and *Subreophax* spp. The Paleocene Cosmopolitan Extinction Taxa (CET; Plate I) are not a major component of the assemblage > 63 µm (< 10 %; Fig. 6), but are common to abundant in the size fraction > 125 µm (> 20 %). Many of these have large, heavily calcified tests. The most common taxa include *Gavelinella beccariiformis*, *Pullenia coryelli* and *Coryphostoma midwayensis* (Table S2). CET such as *Clavulinoides globulifera*, *Cibicidoides dayi* and *Cibicidoides velascoensis* are common in the > 500 µm size fraction, together with trochamminids and large lituolids (Plate I, Figs. 19 and 6–8; Plate IV, Figs. 7 and 8 and 14 and 20). The latter occur up to the top of the Paleocene, but are absent in the Eocene. At −261.5 cm, the Cosmopolitan Extinction Taxa peak at 15 %, their maximum abundance in the studied section (Fig. 6). At the same level, peaks of large, stout, heavily calcified taxa (e.g., *Cibicidoides* and anomalinids) co-occur with agglutinated taxa (*Glomospira*, *Spiroplectammina* and *Haplophragmoides*, Figs. 6 and 7), whereas small, thin-walled forms such as bolivinids, *Siphogenerinoides brevispinosa*

and cibicids decline markedly in relative abundance (Figs. 5–7). Faunal density ($N g^{-1}$), diversity and the percentage abundance of infaunal morphotypes decrease (Fig. 3), as do $\delta^{13}C$ and $CaCO_3$%, whereas the planktonic foraminiferal fragmentation index (F Index) increases significantly (Fig. 3). The upper boundary of this assemblage is defined by the increase in abundance of the opportunists *Tappanina selmensis* and *Siphogenerinoides brevispinosa*, marking the onset of Assemblage B.

3.2 Assemblage B: the pre-CIE Paleocene fauna

Assemblage B occurs at −31 to 0 cm, estimated duration ∼ 34 kyr. At about −20 cm the lithology shifts from reddish to greenish marls with *Zoophycos* and *Chondrites* (intervals Pa I and II of Giusberti et al., 2007). In this assemblage, *Siphogenerinoides brevispinosa* and *Tappanina selmensis* increase in relative abundance compared to Assemblage A (> 10 % at ∼ −27 and −12 cm; Figs. 6 and 7). Between these two peaks (at about ∼ −20 cm), there is a transient negative carbon isotope excursion of about 1 ‰, a drop in $CaCO_3$ from 60 to 40 %, a decline in the coarse fraction to 2 %, and a peak in the F Index (85–90 %; Figs. 3 and 4). Small and thin-walled taxa such as bolivinids, cibicidids and *S. brevispinosa* decrease markedly in relative abundance, whereas big, heavily calcified taxa (e.g. Cosmopolitan Extinction Taxa, *Cibicidoides* spp., *Nuttallides truempyi*) and agglutinated forms increase (Figs. 5–7). In addition, faunal density drops, as does the percentage of infaunal taxa (from 90 to 50 %), and diversity increases (Fig. 3). From −4.5 cm upwards, the preservation of benthic foraminifera deteriorates, while the F Index reaches 100 % (Figs. 3 and 4). At −1.5 cm preservation worsens and most bi-triserial taxa decline in abundance drastically, whereas benthic foraminiferal absolute abundance and $CaCO_3$% both decrease (Fig. 3). Faunal diversity peaks, and anomalinids, *Cibicidoides* spp., *N. truempyi*, *O. umbonatus* as well as agglutinated forms increase markedly in relative abundance (Figs. 3, 5 and 6). In the uppermost Paleocene sample, we see the highest occurrence of most CET (Fig. 6 and Fig. S1). Few CET (e.g., *Aragonia velascoensis*) disappear slightly below this sample,

and they are rare, occurring discontinuously throughout the Paleocene, even in large samples of residue > 125 µm (Fig. S1). The uppermost occurrence of the CET defines the upper boundary of this assemblage, at the base of the black clay layer.

3.3 The black clay

The lowermost Eocene is a thin, black clay layer (0 to +0.3 cm), slightly enriched in organic carbon, and carbonate-free (Giusberti et al., 2007; Figs. 4 and 8). This clay marks the base of the CMU, and contains a few specimens only, agglutinated benthic foraminifera of the genera *Haplophragmoides* and *Recurvoides* (10 specimens in 22 g washed sediment). It probably was deposited over less than a millennium, in view of its small thickness and place within the precessionally paced cycles in the PETM.

3.4 Assemblage C: basal CIE agglutinated fauna

We label this lowermost Eocene interval (lowermost 10 cm of laminated green clays of CMU; estimated duration ∼ 3.5 kyr; Fig. 8) the BFDI (i.e., benthic foraminiferal dissolution interval), sediment with low CaCO$_3$ wt% (∼ 15 %), and the most negative δ^{13}C values in bulk carbonate (−2 ‰). Assemblage C is dominated by agglutinated taxa (about 90 %; Fig. 3) with badly preserved and deformed tests. Tests of calcareous-hyaline forms are rare, partially dissolved and fragmented. Assemblage C has minimum values of faunal density (< 5), diversity, and wt% coarse fraction (Figs. 3 and 4). Infaunal morphogroups have their lowest abundance (ca. 36 %; Fig. 6). Agglutinated foraminifera are mainly represented by *Eobigenerina variabilis* (25 %; Plate 1, Figs. 2 and 3), *Haplophragmoides* spp. (20 %), *Glomospira* spp. (15 %), *Saccamina* spp. (10 %) and *Spiroplectammina navarroana* (∼ 8 %; Plate 2, Fig. 6). In its upper part, Assemblage C has high abundances of *Karrerulina* spp. (∼ 20 %; *K. conversa*; Plate 2, Fig. 4) and *Ammobaculites agglutinans* (10 %; Plate 2, Fig. 1). The latter taxa occur at relatively high abundance in the overlying assemblages, up to ∼ +50–70 cm (Figs. 6 and 7). The up-

per boundary of this assemblage is defined by the first substantial recovery of hyaline taxa (> 50 %).

3.5 Assemblage D: lowermost CIE fauna

In Assemblage D (+10 to +35 cm, lithologically characterized by laminated green clays; estimated duration ∼ 9 kyr; Fig. 8), calcareous-hyaline forms are consistently present and badly preserved, with dominant taxa having dwarfed and thin-walled tests, e.g., *Globocassidulina subglobosa* (25 %), *Tappanina selmensis* (20 %), and *Osangularia* spp. (∼ 11 %; Figs. 6 and 7; Plate 2, Figs. 13–16). From +30 cm upwards, relative abundances of *G. subglobosa* and *Osangularia* spp. drastically declines, whereas *T. selmensis* reaches its maximum abundance (ca. 33 %; Figs. 5 and 7). Minor components are *Bulimina* spp. (10 %), *Pleurostomella* spp., *Oridorsalis umbonatus*, anomalinids and stilostomellids (Fig. 6 and Fig. S2). Agglutinated forms remain abundant, up to 50 %. At +20 cm, calcified radiolarians become abundant, dominating the microfossil association up to +2 m above the base of CMU (Luciani et al., 2007; Figs. 4 and 8). Within the interval of Assemblage D, δ^{13}C shifts from −2 to −1 ‰, and the CaCO$_3$ wt% recovers to ∼ 40 %, despite strong dilution with terrigenous sediments (Fig. 4). The upper boundary of this assemblage is defined by the consistent decrease of *T. selmensis* (to < 5 %).

3.6 Assemblage E: main CIE fauna I

In this interval (+35 to +185 cm; lithologically characterized by green and reddish clays and marls; estimated duration ca. 42 kyr; Fig. 8) benthic foraminiferal preservation improves, and calcareous-hyaline forms dominate the assemblages again (Fig. 3). *Siphogenerinoides brevispinosa* is consistently present again, with two peaks up to 20 % (Figs. 6 and 7). *Pleurostomella* spp. increase to up to > 10 %, and *Bolivinoides crenulata* and smooth-walled *Bolivina* spp. to up to 30–40 % (Figs. 5 and 6). Calcareous-hyaline epifaunals such as cibicids and anomalinids reappear at < 5 % (Fig. 5). Faunal

density and diversity gradually increase upwards, whereas agglutinated taxa markedly decrease in abundance (< 20 %) at ~ +70 cm (Fig. 3). The upper boundary of this assemblage is defined by the marked drop of *S. brevispinosa* (to < 5 %).

3.7 Assemblage F: main CIE fauna II, CIE recovery and post CIE fauna

Assemblage F characterizes the upper half of the CMU (reddish marls), from about +185 cm up to its top (+337.5 cm), and the overlying interval (red marly limestone couplets) up to +649 cm; estimated total duration > 281 kyr; Fig. 8). The relative abundance of *Siphogenerinoides brevispinosa* is low (< 5 %), whereas *Bulimina tuxpamensis* and *Nuttallides truempyi* increase in abundance, respectively to 5 and 10 %, and show cyclical variations in relative abundance (Figs. 6 and 7). Pleurostomellids (~ 10 %), *Bulimina* spp. (~ 10 %), cibicids (~ 10 %), *Oridorsalis umbonatus* (~ 5 %), stilostomellids (~ 5 %) and *Abyssammina* spp. (~ 5 %) are common (Fig. 6). Relative abundance of infaunal taxa (mostly bolivinids) and faunal density ($N g^{-1}$) returns to their Paleocene values (75–80 %; Fig. 3). Diversity increases (simple diversity up to 60, Fisher-α diversity up to 20; Fig. 3) but remains lower than in the Paleocene. All faunal indices show cyclical variation (Fig. 3), as do the relative abundance of benthic foraminifera, and planktic foraminiferal and calcareous nannofossil assemblages (Agnini et al., 2007; Luciani et al., 2007). In the lower third of the interval in which this assemblage occurs, just above the CMU (ca. +337.5 cm), the relative and absolute abundance of radiolarians decrease markedly and agglutinant taxa such as *Glomospira* spp., *Eobigenerina variabilis* and *Karrerulina* spp. slightly increase in relative abundance (~ +2–3 %) (Figs. 3, 4, 6 and 7).

Title Page

Abstract | Introduction

Conclusions | References

Tables | Figures

◄◄ | ►►

◄ | ►

Back | Close

Full Screen / Esc

Printer-friendly Version

Interactive Discussion

4   Discussion: environmental reconstruction

4.1   Paleodepth of the Forada section

Based on benthic foraminifera in the > 125 µm size fraction, Giusberti et al. (2007) suggested a paleodepth between 600 and 1000 m for the Forada section. Our data on the > 63 µm size fraction suggest a somewhat greater paleodepth, i.e. upper lower bathyal, between 1000 and 1500 m (van Morkhoven et al., 1986). Representatives of the bathyal and abyssal Velasco-type fauna (Berggren and Aubert, 1975), such as *Aragonia velascoensis*, *Cibicidoides velascoensis*, *Gyroidinoides globosus*, *Nuttallides truempyi*, *Nuttallinella florealis*, *Osangularia velascoensis* and *Gavelinella beccariiformis* are common at Forada. The faunas across the uppermost PETM interval and higher are similar to the PETM-fauna in the upper abyssal Alamedilla section (Souther Spain; Alegret et al., 2009) and at Walvis Ridge at 1500 m paleodepth (Thomas and Shackleton, 1996; Thomas, 1998). *Abyssammina* spp. and *Nuttallides truempyi* (upper depth limit at 1000 and 300 m respectively; Van Morkhoven et al., 1986; Speijer and Schmitz, 1998) increase in abundance by more than a factor of 2 during the PETM at Forada, as typical for PETM deep-sea benthic foraminiferal records (e.g., Thomas, 1998, 2007; Thomas and Shackleton, 1996; Alegret et al., 2009a, 2011; Giusberti et al., 2009). In these deliberations we excluded the bolivinids, because we consider that their high abundance is due to the "delta depression effect" (see below).

4.2   The Paleocene

4.2.1   The Belluno Basin deep-sea environment in the late Paleocene (Assemblage A)

Throughout most of the investigated section, infaunals strongly dominate over epifaunals, mainly due to the high abundances of bolivinids (Figs. 3 and 5). Such dominance of bolivinids is common in lower and middle Eocene hemipelagic Scaglia sediments

in the Belluno basin (Agnini et al., 2009; Boscolo Galazzo et al., 2013). Presently, bolivinids are common along continental margins, and at bathyal depths, at the interception of the oxygen minimum zone with the seafloor. High abundances of bolivinids commonly correlate with high organic matter flux and/or oxygen depletion (e.g., Murray, 1991; Gooday, 1994; Bernhard and Sen Gupta, 1999; Schmiedl et al., 2000; Thomas et al., 2000; Jorissen et al., 1995, 2007; Thomas, 2007). We see high abundances of such taxa typically at greater depths than usual in regions with significant organic matter input from rivers, the so-called "delta-depression" effect first described in the Gulf of Mexico (Pflum and Frerichs, 1976; Jorissen et al., 2007). Such lateral inputs of organic matter thus result in (partial) decoupling between the food supply to the benthos and local primary productivity (e.g., Fontanier et al., 2005; Arndt et al., 2013).

At Forada, there is neither geochemical nor sedimentological evidence for persistent suboxic conditions at the sea-floor (Giusberti et al., 2007), and the high benthic foraminiferal faunal diversity likewise does not indicate low oxygen conditions. The upper Paleocene calcareous plankton is dominated by morozovellids indicating oligotrophic surface water conditions (Luciani et al., 2007; Fig. 8). The calcareous nannofossil assemblage is dominated by the generalist taxa *Toweius* and *Coccolithus*, with high percentages of *Sphenolithus* and *Fasciculithus* (Agnini et al., 2007; Fig. 8), supporting that surface waters were oligotrophic. We thus think that environments in the Belluno Basin, close to a continental margin (Agnini et al., 2007), were characterized by the "delta depression effect", in which hemipelagic sedimentation incorporated significant laterally transported terrigenous organic matter to serve as food for the benthos (e.g., Fontanier et al., 2008; Arndt et al., 2013).

The occurrence of large, epifaunal ($> 500\,\mu m$) species (Assemblage A and B), has been related to an optimum food supply, but also to very low food supply, since a lack of food keeps individuals from reproducing successfully and leads to continued testgrowth (Boltovskoy et al., 1991; Thomas and Gooday, 1996). The relative abundance of these Paleocene cosmopolitan extinction taxa is not high (average $\sim 5\,\%$; Fig. 6) due to the abundance of small bolivinids. In other deep-water PETM sections, buliminids

Benthic foraminifera at the Paleocene/Eocene thermal maximum

L. Giusberti et al.

Title Page

Abstract | Introduction

Conclusions | References

Tables | Figures

◀◀ | ▶▶

◀ | ▶

Back | Close

Full Screen / Esc

Printer-friendly Version

Interactive Discussion

and uniserial calcareous taxa may dominate the $> 63\,\mu m$ fraction (e.g., Thomas, 2003; Giusberti et al., 2009).

Overall, Assemblage A, in agreement with data on calcareous plankton (Fig. 8), indicates oligo-mesotrophic surface waters, with bolivinids probably exploiting refractory, laterally advected organic matter. The high faunal diversity suggests that seasonal to periodical increases in primary productivity may have occurred, allowing a species-rich, highly diverse infauna and epifauna to inhabit the sea-floor, and co-occur with the bolivinids in the sedimentary record.

4.2.2 The latest Paleocene: precursor climate change (Assemblage B)

The onset of Assemblage B, about 34 kyr before the onset of the CIE ($\sim -30\,cm$), is marked by increase in relative abundance of opportunistic taxa such as *Tappanina selmensis* and *Siphogenerinoides brevispinosa* (Figs. 6 and 7). The arrival of *Tappanina selmensis,* previously an upper bathyal to outer shelf species (Frenzel, 2000), might indicate warming of deep waters before the beginning of the PETM, as also reflected in the migration of warm-water planktonic species to high southern latitudes (Thomas and Shackleton, 1996). The benthic foraminiferal changes roughly coincided with a significant increase in acarininids% ($> 50\,\%$), likely indicating warming of surface waters (Luciani et al., 2007). The foraminiferal assemblages hence suggest warming throughout the water column, and increased surface nutrient availability and deep-water food availability, whereas no changes in productivity in calcareous nannofossils are recorded (Agnini et al., 2007; Luciani et al., 2007; Fig. 8). The foraminiferal evidence for warming is associated with an increase in $\delta D_{n\text{-alkanes}}$ and TEX_{86} values (Fig. 10), suggesting increased aridity and sea surface temperature prior to the onset of the CIE (Tipple et al., 2011).

Multiple proxies thus indicate that climatic and oceanographic conditions started to change $\sim 30\,kyr$ before the onset of the CIE, pointing to a PETM precursor event, reflected by a $< 5\,cm$ thick dissolution interval at $\sim -22\,cm$, coinciding with a negative shift in bulk $\delta^{13}C$ ($-1\,\permil$; Figs. 3 and 4). Within this interval dissolution-sensitive ben-

thic foraminifera (e.g., *S. brevispinosa* and small bolivinids) markedly decrease in abundance, while more robust and agglutinant taxa increase (Figs. 3 and 5–8), as does the F Index of planktic foraminifera (to ∼ 85–90 %; Luciani et al., 2007; Fig. 4). This dissolution level may thus reflect a brief episode of rising lysocline/CCD (< 5 kyr) in response to a precursory emission of isotopically light carbon (Bowen et al., 2015). Similar precursor events have been observed worldwide (e.g., Sluijs et al., 2007b, 2011; Secord et al., 2010; Kraus et al., 2013; Garel et al., 2013; Bornemann et al., 2014; Bowen et al., 2015), indicating that disturbance of the global carbon cycle started before the PETM, as potentially also reflected in the occurrence of hyperthermals in the Paleocene (Thomas et al., 2000; Cramer et al., 2003; Coccioni et al., 2012).

At the top of Assemblage B (uppermost 4.5 cm), just prior to the onset of the CIE, carbonate preservation declined markedly, as reflected in F Index, CaCO$_3$%, and foraminiferal preservation. In this interval representing the "burndown" layer (BL; e.g., Thomas and Shackleton, 1996; Thomas et al., 1999; Giusberti et al., 2007; Figs. 7 and 8 and Fig. S1) CET remained present. Dissolution in the upper BL removed most thin, dissolution-prone calcareous tests (e.g., *Siphogenerinoides brevispinosa* and small bolivinids), concentrating the more heavily calcified and the agglutinated taxa (included CET; Figs. 5–7). Benthic foraminiferal assemblages in the topmost Paleocene at Forada thus cannot be interpreted with confidence due to the severe dissolution.

4.3 The PETM: climate and marine life during the Cenozoic warmest time

4.3.1 The black clay: a desert below the CCD

This very thin, carbonate-free interval is somewhat enigmatic. The virtually barren sediment may have been deposited during the maximum rise of the CCD, under environmental conditions so unfavorable that benthic life was excluded, a "dead-zone" (*sensu* Harries and Kauffman, 1990) during the earliest phase of the PETM. Geochemical redox indices in the black clay and the underlying and overlying samples suggest persistently oxygenated bottom waters (Giusberti et al., 2007), but may reflect diagenesis

during re-oxygenation of bottom waters after a short period of anoxia, as commonly observed for Mediterrean sapropels (Higgs et al., 1994; van Santvoort et al., 1996). The presence of the thin black clay without microfossils thus is highly suggestive of a brief pulse of anoxia, as supported by a single peak value of organic carbon (0.6 wt%; Giusberti et al., 2007). The high value of biogenic barium (3151 ppm) in the black clay (Fig. 4), despite the fact that barite is generally not preserved under anoxic conditions (Paytan and Griffith, 2007; Paytan et al., 2007) may represent reprecipitation at the oxic/anoxic sediment interface after dissolution under anoxic conditions (Giusberti et al., 2007), and/or high rates of organic remineralization in the water column, during which the barite forms (Ma et al., 2014).

4.3.2 Climate and life during the early peak PETM (Assemblages C and D)

The 10 cm of sediment directly overlying the Paleocene/Eocene boundary (i.e. the base of the CIE; Figs. 7 and 8) was deposited in strongly $CaCO_3$-corrosive waters, close to or below the CCD. The rapid rise of the CCD/lysocline during the PETM is a predicted consequence of massive input of carbon (CO_2 or CH_4) in the ocean–atmosphere system on a millennial timescale (e.g., Dickens et al., 1997; Thomas, 1998; Zachos et al., 2005; Zeebe et al., 2009, 2014; Hoenisch et al., 2012). The carbonate dissolution at Forada is consistent with observations at many other deep-sea sites (e.g., Schmitz et al., 1997; Thomas, 1998; Zachos et al., 2005; Kelly et al., 2010). The benthic foraminiferal extinction event (BEE) at Forada (i.e., the BB1/BB2 zonal boundary of Berggren and Miller, 1989) occurs within this 10 cm-thick interval, between the top of the CET-bearing burndown layer and the base of Assemblage D, where benthic calcareous taxa reappear (Figs. 7 and 8 and Fig. S1). The concentration of CET in BL, and the reappearance of calcareous hyaline taxa only 10 cm above the onset of the PETM at Forada, confirms that the CET extinction occurred over 3.5 kyr or less in the central western Tethys.

Sediment just above the black clay, reflecting a first slight deepening of the CCD, contains a low diversity, pioneer fauna of mostly agglutinant, dwarfed (close to 63 μm in size) benthic foraminifera. This first wave of pioneer taxa recolonized the sea-floor

during the peak-CIE, in CaCO$_3$-undersaturated waters, and reflects a highly stressed environment (Assemblage C; Figs. 6–8). Calcareous nannofossil assemblages present sign of dissolution, while planktic foraminifera are virtually absent (Agnini et al., 2007; Luciani et al., 2007; Fig. 8).

5 After ca. 4 kyr, further deepening of CCD allowed a consistent increase in abundance of benthic calcareous taxa (ca. 50 %; Assemblage D; Fig. 3), including dwarfed and thin-walled forms of *G. subglobosa, Tappanina selmensis, Osangularia* spp. and *Oridorsalis umbonatus* (Figs. 6 and 7). The apparence of these calcareous recolonizers coincides with the lowermost recovery of bulk carbonate δ^{13}C values, from −2

10 to −1‰ (Giusberti et al., 2007; Tipple et al., 2011; Fig. 7). Assemblage D contains almost equal abundances of calcareous and agglutinant taxa, indicating that factors other than bottom water CaCO$_3$ concentration were controlling faunal variability within this assemblage (Figs. 6 and 7). Possibly, strongly enhanced runoff and sediment delivery can explain the abundance of agglutinated taxa (40–60 %), such as *Glomospira*

15 spp. (e.g., Arreguin-Rodriguez et al., 2013), above the first 10 cm of the CMU. We thus recognize a rapid succession of recolonizer taxa during the first 12 kyr of the CIE (Assemblages C–D). The small size of both the agglutinant and hyaline recolonizers is indicative of r-strategist species which reproduce quickly thus can quickly repopulate stressed environments, as soon as conditions improve slightly (e.g., Koutsoukos

20 et al., 1990; Thomas, 2003). The rapid pace at which different populations of recolonizers succeeded each other indicates a highly unstable environment, with marked fluctuations in the amount and quality of the food reaching the sea floor. Sediment deposition during this interval may have occurred in rapid pulses, e.g., following intense rainstorms, carrying refractory organic matter to the deep-sea environment. Pauses

25 between events may have allowed the benthic foraminifera to recolonize the sediment, profiting of the abundance of food. This is consistent with calcareous nannofossil assemblages showing an increase in *Ericsonia* and declines in abundance of *Sphenolithus*, *Octolithus*, *Zygrablithus* and *Fasciculithus*, indicating an unstable and nutrient rich upper water column (Agnini et al., 2007; Fig. 8). Archaeal biomarkers show a large

Benthic foraminifera at the Paleocene/Eocene thermal maximum

L. Giusberti et al.

Title Page

Abstract | Introduction

Conclusions | References

Tables | Figures

◀ | ▶

◀ | ▶

Back | Close

Full Screen / Esc

Printer-friendly Version

Interactive Discussion

influx of terrestrial, soil-derived organic matter (Branched and Isoprenoid Tetraethers or BIT Index) from the onset of the PETM up to ∼ +10 cm (Tipple et al., 2011). Higher plant *n*-alkane average chain length (ACL) decreased immediately after the onset of the CIE, consistent with increased humidity (Fig. 9; Tipple et al., 2011). The abundance
5 of the clay mineral chlorite indicates enhanced physical erosion (Robert and Kennett, 1994) during deposition of the lower 50 cm of the CMU, rapidly decreasing upward (Fig. S4).

The greenish marly clays containing Assemblages C and D show primary lamination, indicating that macrobenthic invertebrates were absent, as at Dee and Mead Stream
10 sections (New Zealand; Nicolo et al., 2010), and Zumaya (Spain; Rodriguez-Tovar et al., 2011). The presence of benthic foraminifera, however, indicates that bottom and pore waters were not permanently anoxic. Pore waters may have become dysoxic periodically due to high temperatures, decomposing organic matter and possibly enhanced water column stratification, leading to the absence of metazoans and stressed benthic
15 foraminiferal assemblages.

4.3.3 Climate and deep sea life during the core of the CIE and Recovery (Assemblages E, F)

The benthic foraminiferal assemblage changes significantly from Assemblage D to Assemblage E. Bolivinids return as a major faunal component (50 %), and agglutinants
20 decrease in abundance. Peaks of tapered elongate calcareous forms, including *Siphogenerinoides brevispinosa*, buliminids, pleurostomellids and stilostomellids, replace the recolonizers. These groups could have been opportunist taxa, able to flourish when food supply was periodically high. Coinciding with Assemblage E, planktic foraminifera return to be a significant component of the microfossil assemblage (e.g., Luciani et al.,
25 2007; Fig. 8), while radiolarians remain abundant throughout the CMU (Giusberti et al., 2007; Luciani et al., 2007). The planktic foraminiferal assemblage is dominated by acarininids, with a double peak of the excursion species *Acarinina sibayaensis* and *A. africana*, which, combined with the high percentages of the nannofossil *Ericsonia*,

Benthic foraminifera at the Paleocene/Eocene thermal maximum

L. Giusberti et al.

indicate warm and eutrophic surface waters (Agnini et al., 2007; Luciani et al., 2007; Fig. 8).

Detrital hematite sharply increased in concentration at the onset of Assemblage E (Giusberti et al., 2007; Dallanave et al., 2010, 2012; Fig. 4). Hematite forms in soils under warm and dry conditions, and an increase of hematite in marine sediments is considered indicative of an arid climate over the adjoining land and increased wind strength (Larrasoaña et al., 2003; Zhang et al., 2007; Itambi et al., 2009), or humid to subhumid climates with seasonal drying (Torrent et al., 2006). It is delivered to the deep sea environment through river runoff or as aeolian dust (e.g., Zhang et al., 2007; Itambi et al., 2009). Within the CMU, hematite shows cyclical fluctuations with a ~ 21 kyr periodicity, but other terrigenous components (quartz and phyllosilicates) do not co-vary in abundance after a $\sim 15\%$ increase at the onset of the CMU (Fig. 4). To explain the different abundance patterns we interpret hematite as wind-delivered, silicate minerals as runoff-delivered.

The hematite% peaks may be indicative of cyclical variability in wind-delivered material, rather than the earlier prevailing consistently humid climate. The lithological anomaly of the CMU, the fivefold increase in sedimentation rates and increase in reworked Cretaceous nannofossils (Agnini et al., 2007; Fig. 8), as well as the silicate mineral and hematite% records all indicate marked fluctuations in the hydrological regime throughout this interval. High hematite% may reflect the presence of high-pressure cells over land, during an overall dry climate phase, with increased wind strength and dust delivery to the sea. In contrast, low values of hematite% may indicate periods of greater humidity and enhanced precipitation. Such alternation of wet and arid phases favored deeper soil erosion on the continental areas surrounding the Belluno basin (Thiry, 2000; Schmitz and Pujalte, 2003), causing major washouts during the wet phases, which may explain the fivefold increase in sedimentation rates and 15% increase in phyllosilicate abundance in the CMU (Fig. 4).

The hematite% cycles are in phase with cycles in CaCO$_3$%, radiolarian abundance, and bulk carbonate δ^{13}C, slightly preceding the others stratigraphically (Fig. 4). During

Full Screen / Esc

the arid climate phase, enhanced wind strength may have generated intense surface water mixing and offshore nutrient upwelling, inducing increases in primary productivity and phytoplankton blooms. The blooms in primary productivity resulted in deposition of abundant algal biomass, leading to the occurrence of peaks of pleurostomellids, stilostomellids and *Siphogenerinoides brevispinosa* in Assemblage E. Productivity may have remained fairly high during the wet periods, as indicated by consistently high biogenic barium throughout the CMU (Giusberti et al., 2007; Paytan et al., 2007). During the rainy periods upwelling rates may have been lower, with nutrients mostly supplied in river runoff. The delivery of food to the seafloor may have been more continuous, but with more important input of refractory organic matter from land.

In contrast to these proxies which show cyclity at precessional periods throughout the CMU, higher plant *n*-alkane average chain length (ACL) and δD vary only in its lowermost 50 cm (Tipple et al., 2011; Fig. 9). Possibly, the sedimentary *n*-alkanes were derived from a pool of plant material produced during subsequent wet and dry phases, so that ACL and δD may represent averaged records of leaf wax *n*-alkanes produced during different mean climate states in the upper CMU. Even so, the δD values within the CMU are on average ~ 15‰ lower than above and below (Fig. 9), as reported for the Cicogna section (10 km away; Krishnan et al., 2015), possibly reflecting more humid conditions/higher precipitation during the PETM wet times (e.g., Sachse et al., 2006; Smith and Freeman, 2006), or greater productivity of plant material during the wet phases. Alternatively, it may reflect a primary change in the isotopic composition of meteoric waters (Krishnan et al., 2015).

In the following benthic foraminiferal Assemblage F (upper CMU, recovery phase), *Siphogenerinoides brevispinosa* and *Tappanina selmensis* are less abundant, whereas *Bulimina tuxpamensis*, *Abyssammina* spp., and *Nuttallides truempyi* increase in relative abundance (Figs. 6 and 7). These are typical deep-sea, open-ocean taxa which thrive under more oligotrophic conditions (e.g., Thomas, 1998), and might indicate progressively less intense or shorter primary productivity blooms during the arid phases, and/or mark the return to fully oxygenated sea-floor and pore water conditions. Less intense

Benthic foraminifera at the Paleocene/Eocene thermal maximum

L. Giusberti et al.

eutrophy at the transition from Assemblage E to F is further supported by calcareous plankton data, showing a decrease in the planktic foraminiferal excursion species, and among nannofossils, a decrease in *Ericsonia* (Agnini et al., 2007; Luciani et al., 2007; Fig. 8). Conciding with the top of the CMU, there were marked changes in calcareous plankton assemblages, although benthic foraminiferal Assemblage F persisted. Among calcareous nannofossils the abundance of *Zygrablithus*, *Sphenolithus* and *Octolithus* increased, whereas that of reworked taxa decreased. In the planktic foraminiferal assemblage, *Acarinina* species declined in abundance, and the fauna became more diverse, with fluctuations modulated by lithology in the marl-limestone couplets overlying the CMU (Fig. 8).

The lithological unit above the CMU consists of an alternation of limestones and marls at precessional frequencies (~ 21 kyr; Fig. 3). These limestone-marl couplets persist for up to 8 m above the CMU (Giusberti et al., 2007; Luciani et al., 2007), then gradually become less clearly expressed, fading upwards. The marl-limestone couplets may reflect the persistence of wet (marl)-arid (limestone) cycles for ~ 800 kyr after the end of the CMU deposition, though at an amplitude declining over time. Our benthic foraminiferal data agree with this interpretation, showing substantially unchanged seafloor conditions up to +650 cm (uppermost sample analyzed).

Intense weather extremes during the PETM are being increasingly documented at mid to subtropical latitudes (Fig. 1; Table S1). The long-lasting cyclity recorded at Forada suggests that this enhanced variability may have lasted for several hundred of thousand years after the onset of the CIE. These weather extremes persisting over 10^5 kyr may have significantly enhanced the rate of erosion and weathering, through the occurrence of alternating wet-dry periods. The weathering may have influenced atmospheric CO_2 levels, by consumption of CO_2 during weathering reactions and their effect on the carbon cycle. The increased supply of cations through enhanced weathering-erosion would have driven ocean pH up, and CO_2 down (Broecker and Peng, 1982; Raymo et al., 1988; Zachos et al., 2005). Enhanced seasonal extremes across large geographical areas (the subtropical to mid latitudinal belt) thus might have

been a response to the large CO_2 input at the Paleocene–Eocene transition, and may have had a primary role in restoring the carbon cycle to steady state.

5 Conclusions

The continuous and expanded record of benthic foraminifera across the PETM at Forada, integrated with the extensive datasets earlier generated across this interval, may provide the most complete reconstruction of ecological and climatic changes during the Paleocene/Eocene thermal maximum in Europe. Coupled sedimentological, molecular and micropaleontological records highlight a complex sequence of environmental and climatic changes during the time period across the CIE. Climatic and oceanographic conditions started to change ∼ 30 kyr before the onset of the PETM, during a possible precursor event, as also observed elsewhere (e.g., Bowen et al., 2015).

Our high-resolution benthic foraminiferal record combined with the established chronology lets us infer that the BEE in the central-western Tethys occurred over a time interval of not more than 4 kyr. At the onset of the PETM, combined de-oxygenation, acidification and environmental instability may have synergistically impacted deep sea life, with a locally brief pulse of anoxia (probably < 1000 yr), resulting in a "dead zone" (black clay). Within the following CMU (coinciding with the main phase of the CIE), 4 benthic foraminiferal assemblages occurred (C–E and lower F). Assemblage C, following the "dead zone" is characterized by successive peaks of different agglutinant recolonizers. Calcareous pioneer forms return in the following Assemblage D, after calcium carbonate saturation increased. The complex succession of peaks of agglutinant and hyaline recolonizers in these two assemblages (C, D; 12.5 kyr), suggests multiple repopulation episodes during major environmental instability. The benthic foraminiferal data integrated with molecular and mineralogical data point to increased precipitation and strong continental erosion during this short initial stage of the PETM, leading to pulses of massive sediment discharge.

Title Page

Abstract | Introduction

Conclusions | References

Tables | Figures

◄ | ►►

◄ | ►

Back | Close

Full Screen / Esc

Printer-friendly Version

Interactive Discussion

Within the core of the CIE, above this interval of wet climate, δ^{13}C and mineralogical properties such as hematite and calcium carbonate wt% vary at precessional periodicity. Combined with data on radiolarian abundance and benthic foraminiferal assemblage composition this variability suggests an alternation of overall wetter and drier periods. Higher rates of erosion and sediment discharge during the wet periods favored benthic foraminifera such as bolivinids, whereas enhanced wind-driven upwelling during the dry periods triggered algal blooms, favoring taxa such as pleurostomellids, abyssamminids, *Siphogenerinoides brevispinosa*, *Bulimina tuxpamensis*, and epifaunal taxa.

Enhanced weather extremes during most of the PETM may have led to a decrease in total precipitation over the central western Tethys. During the overall wetter periods, however, the rainy seasons were wetter, similar to the strengthened seasonality inferred for subtropical and mid latitudes (Table S1).

The benthic foraminiferal assemblage at Forada did not significantly change with the onset of the deposition of marl-limestone couplets unit above the CMU (mid and upper third of Assemblage F). The occurrence of marl-limestone couplets combined with this lack of change in benthic assemblages suggests that the enhanced climatic variability at precessional timescales persisted well after the end of the CIE recovery. We argue that emphasized seasonal extremes at mid-latitudes might have been a direct climate response to the huge CO_2 input at the Paleocene–Eocene transition, and may have had a primary role in restoring carbon cycle steady state through links with the water cycle and weathering rates.

The Supplement related to this article is available online at doi:10.5194/cpd-11-4205-2015-supplement.

References

Agnini, C., Fornaciari, E., Rio, D., Tateo, F., Backman, J., and Giusberti, L.: Response to calcareous nannofossil assemblages, mineralogy and geochemistry to the environmental perturbations across the Paleocene/Eocene boundary in the Venetian Pre-Alps, Mar. Micropaleontol., 63, 19–38, 2007.

Agnini, C., Macrì, P., Backman, J., Brinkhuis, H., Fornaciari, E., Giusberti, G., Luciani, V., Rio, D., Sluijs, A., and Speranza, F.: An early Eocene carbon cycle perturbation at ~ 52.5 Ma in the Southern Alps: chronology and biotic response, Paleoceanography, 24, PA2209, doi:10.1029/2008PA001649, 2009.

Alegret, L., Molina, E., and Thomas, E.: Benthic foraminiferal faunal turnover across the cretaceous/tertiary boundary at Agost (Southeastern Spain), Mar. Micropaleontol., 48, 251–279, 2003.

Alegret, L., Ortiz, N., and Molina, E.: Extinction and recovery of benthic foraminifera across the Paleocene–Eocene thermal maximum at the Alamedilla section (Southern Spain), Palaeogeogr. Palaeocl., 279, 186–200, 2009a.

Alegret, L., Ortiz, S., Orue-Extebarria, X., Bernaola, G., Baceta, J. I., Monechi, S., Apellaniz, E., Pujalte, V.: The Paleocene–Eocene thermal maximum: new data on microfossil turnover at the Zumaia section, Spain, Palaios, 24, 318–328, 2009b.

Alegret, L., Ortiz, S., Arenillas, I., and Molina, E.: What happens when the ocean is overheated? The foraminiferal response across the Paleocene–Eocene thermal maximum at the Alamedilla section (Spain), Geol. Soc. Am. Bull., 122, 1616–1624, 2010.

Alve, E. and Goldstein, S. T., Propagule transport as a key method of dispersal in benthic foraminifera (protists), Limnol. Oceanogr., 48, 2163–2170, 2003.

Arndt, S., Jørgense, B. B., LaRowe, D. E., Middeburg, J. J., Pancost, R. D., and Regnier, P., Quantifying the degradation of organic matter in marine sediments: a review and synthesis, Earth-Sci. Rev., 123, 53–86, 2013.

Title Page

Abstract | Introduction

Conclusions | References

Tables | Figures

|◀ | ▶|

◀ | ▶

Back | Close

Full Screen / Esc

Printer-friendly Version

Interactive Discussion

Arreguín-Rodríguez, G. J., Alegret, L., and Ortiz, S.: *Glomospira* acme during the Paleocene–Eocene thermal maximum: response to $CaCO_3$ dissolution or to ecological forces?, J. Foramin. Res., 43, 37–49, 2013.

Arreguín-Rodríguez, G. J., Alegret, L., Sepúlveda, J., Newman, S., and Summons, R. E.: Enhanced terrestrial input supporting the *Glomospira* acme across the Paleocene–Eocene boundary in Southern Spain, Micropaleontology, 60, 43–51, 2014.

Aubry, M.-P., Ouda, K., Dupuis, C., Berggren, W. A., Van Couvering, J. A., Ali, J., Brinkhuis, H., Gingerich, P. R., Heilmann-Clausen, C., Hooker, J., Kent, D. V., King, C., Knox, R. W. O. B., Laga, P., Molina, E., Schmitz, B., Steurbaut, E., and Ward, D. R.: The global standard stratotype-section and point (GSSP) for the base of the Eocene series in the Dababiya section (Egypt), Episodes, 30, 271–286, 2007.

Aze, T., Pearson, P. N., Dickson, A. J., Badger, M. P. S., Bown, P. R., Pancost, R. D., Gibbs, S. J., Huber, B. T., Leng, M. J., Coe, A. L., Cohen, A. S., and Foster, G. L.: Extreme warming of tropical waters during the Paleocene–Eocene thermal maximum, Geology, 42, 739–742, 2014.

Bains, S., Corfield, R. M., and Norris, R. D.: Mechanisms of climate warming at the end of the Paleocene, Science, 285, 724–727, doi:10.1126/science.285.5428.724, 1999.

Beckmann, J. P.: Distribution of benthonic foraminifera at the Cretaceous–Tertiary boundary of Trinidad (West Indies), in: Part 5: The Cretaceous–Tertiary boundary, International Geological Congress Report, 21 Session Norden, Copenhagen, 57–59, 1960.

Berggren, W. A. and Aubert, J.: Paleocene benthonic foraminiferal biostratigraphy, paleobiogeography and paleoecology of Atlantic-Tethyan regions: midway type fauna, Palaeogeogr. Palaeocl., 18, 73–192, 1975.

Berggren, W. A. and Miller, K. G.: Cenozoic bathyal and abyssal calcareous benthic foraminiferal zonation, Micropaleontology, 35, 308–320, 1989.

Bernhard, J. M. and Sen Gupta, B. K.: Foraminifera of oxygen deplete environments, in: Modern Foraminifera, edited by: Sen Gupta, B. K., Kluwer Academic Publishers, Dordrecht, 201–216, 1999.

Boltovskoy, E., Scott, D. B., and Medioli, F. S.: Morphological variations of benthic foraminiferal tests in response to changes in ecological parameters; a review, J. Paleontol., 65, 175–185, 1991.

Benthic foraminifera at the Paleocene/Eocene thermal maximum

L. Giusberti et al.

Bornemann, A., Norris, R. D., Lyman, J. A., D'haenens, S., Groeneveld, J., Röhl, U., Farley, K. A., and Speijer, R. P.: Persistent environmental change after the Paleocene–Eocene thermal maximum in the eastern North Atlantic, Earth Planet. Sc. Lett., 394, 70–81, 2014.

Boersma, A: Oligocene and other Tertiary benthic foraminifers from a depth traverse down Walvis Ridge, Deep Sea Drilling Project Leg 74, Southeast Atlantic, Initial Rep. Deep Sea, 75, 1273–1300, doi::10.2973/dsdp.proc.75.150.1984, 1984.

Boscolo Galazzo, F., Giusberti, L., Luciani, V., and Thomas, E.: Paleoenvironmental changes during the Middle Eocene climatic optimum (MECO) and its aftermath: the benthic foraminiferal record from the Alano section (NE Italy), Palaeogeogr. Palaeocl., 378, 22–35, 2013.

Boscolo-Galazzo, F., Thomas, E., and Giusberti, L.: Benthic foraminiferal response to the Middle Eocene climatic optimum (MECO) in the Southeastern Atlantic (ODP Site 1263), Palaeogeogr. Palaeocl., 417, 432–444, 2015.

Bowen, G. J., Beerling, D. J., Koch, P. L., Zachos, J.C, Quattlebaum, T.: A humid climate state during the Palaeocene/Eocene thermal maximum, Nature, 432, 495–499, 2004.

Bowen, G. J., Maibauer, B. J., Kraus, M. J., Roehl, U., Westerhold. T., Steike, A., Gingerich, P. D., Wing, S. L., and Clyde, W. J.: Two massive, rapid release of carbon during the onset of the Palaeocene–Eocene thermal maximum, Nat. Geosci., 8, 44–47, 2015.

Braga, G., De Biase, R., Gruning, A., and Proto Decima, F.: Foraminiferi bentonici del Paleocene e dell'Eocene della sezione di Possagno, in: Monografia micropaleontogica sul Paleocene e l'Eocene di Possagno, Provincia di Treviso, Italia, edited by: Bolli, H. M., Schweizerische Paläontologische Abhandlungen, Abhandlungen, Basel, 97, 85–111, 1975.

Bralower, T. J.: Evidence of surface water oligotrophy during the Paleocene–Eocene thermal maximum: nannofossil assemblage data from Ocean Drilling Program Site 690, Maud Rise, Weddell Sea, Paleoceanography, 17, 1023, doi:1029/2001PA000662, 2002.

Broecker, W. S. and Peng, T.- H.: Tracers in the Sea, Palisades, Eldigio Press, New York, 690 pp., 1982.

Buzas, M. A., Culver, S. J., and Jorissen, F. J.: A statistical evaluation of the microhabitats of living (stained) infaunal benthic foraminifera, Mar. Micropaleontol., 29, 73–76, 1993.

Cetean, C., Setoyama, E., Kaminski, M. A., Neagu, T., Bubík, M., Filipescu, S., and Tyszka, J.: *Eobigenerina*, n. gen., a cosmopolitan deep-water agglutinated foraminifer, and remarks on species formerly assigned to the genera *Pseudobolivina* and *Bigenerina*, in: Eight International Workshop on Agglutinated Foraminifera, Abstract Volume, edited by: Filipescu, S. and

Kaminski, M. A., Grzybowski Foundation Special Publication, Presa Universitară Clujeană, Romania, 14, 6–7, 2008a.

Cetean, C., Bălci, R., Kaminski, M. A., and Filipescu, S.: Biostratigraphy of the cenomanian-turonian boundary in the Eastern Carpathians (Dâmboviţa Valley): preliminary observations, Stud. Univ. Babeş-Bol., Geologia, 53, 11–23, 2008b.

Cetean, C., Setoyama, E., Kaminski, M. A., Neagu, T., Bubík, M., Filipescu, S., and Tyszka, J.: *Eobigenerina*, a cosmopolitan deep-water agglutinated foraminifer, and remarks on late Paleozoic to Mesozoic species formerly assigned to *Pseudobolivina* and *Bigenerina*, in: Proceedings of the Eight International Workshop on Agglutinated Foraminifera, edited by: Filipescu, S. and Kaminski, M. A., Grzybowski Foundation Special Publication, Grzybowski Foundation Special Publication, Presa Universitară Clujeană, Romania, , 16, 19–27, 2011.

Chun, C. O. J, Delaney, M. L., and Zachos, J. C.: Paleoredox changes across the Paleocene–Eocene thermal maximum, Walvis Ridge (ODP sites 1262, 1263, and 1266): evidence from Mn and U enrichment factors, Paleoceanography, 25, PA4202, doi:10.1029/2009PA001861, 2010.

Coccioni, R. and Galeotti, S.: Orbitally induced cycles in benthic foraminiferal morphogroups and trophic structure distribution patterns from the late Albian "Amadeus Segment" (Central Italy), J. Micropalaeontol., 12, 227–239, 1993.

Coccioni, R., Bancala, G., Catanzariti, R., Fornaciari, E., Frontalini, F., Giusberti, L., Jovane, L., Luciani, V., Savian, J., and Sprovieri, M.: An integrated stratigraphic record of the Palaeocene-lower Eocene at Gubbio (Italy): new insights into the early Palaeogene hyperthermals and carbon isotope excursions, Terra Nova, 45, 380–386, 2012.

Collinson, M. E., Steart, D. C., Scott, A. C., Glasspool, I. J., and Hooker, J. J.: Episodic fire, runoff and deposition at the Palaeocene–Eocene boundary, J. Geol. Soc. London, 164, 87–97, 2007.

Colosimo, A. B., Bralower, T. J., and Zachos, J. C.: Evidence of lysocline shoaling at the Paleocene/Eocene Thermal Maximum on Shatsky Rise, northwest Pacific, Proceedings of the Ocean Drilling Program, Scientific Results, 198, College Station, Texas, 1–36, 2006.

Corliss, B. H.: Microhabitats of benthic foraminifera within deep-sea sediments, Nature, 314, 435–438, 1985.

Corliss, B. H. and Chen, C.: Morphotype patterns of Norwegian Sea deep-sea benthic foraminifera and ecological implications, Geology, 16, 716–719, 1988.

Title Page

Abstract | Introduction

Conclusions | References

Tables | Figures

◀◀ | ▶▶

◀ | ▶

Back | Close

Full Screen / Esc

Printer-friendly Version

Interactive Discussion

Cramer, B. S., Wright, J. D., Kent, D. V., and Aubry, M.-P.: Orbital climate forcing of δ^{13}C excursions in the late Paleocene-early Eocene (chrons C24n-C25n), Paleoceanography, 18, 1097, 2003.

Crouch, E. M., Dickens, G. R., Brinkhuis, H., Aubry, M.-P., Hollis, C. J., Rogers, K. M., and Visscher, H.: The *Apectodinium* acme and terrestrial discharge during the Paleocene–Eocene thermal maximum: new palynological, geochemical and calcareous nannoplankton observations at Tawanui, New Zealand, Palaeogeogr. Palaeocl., 194, 387–403, 2003.

Dallanave, E., Tauxe, L., Muttoni, G., and Rio, D.: Silicate weathering machine at work: rock magnetic data from the late Paleocene–early Eocene Cicogna section, Italy, Geochem. Geophy. Geosy., 11, Q07008, doi:10.1029/2010GC003142, 2010.

Dallanave, E., Muttoni, G., Agnini, C., Tauxe, L., and Rio, D.: Is there a normal magnetic-polarity event during the Palaeocene–Eocene thermal maximum ($\sim$ 55 Ma)? Insights from the palaeomagnetic record of the Belluno Basin (Italy), Geophys. J. Int., 191, 517–529, 2012.

DeConto, R. M., Galeotti, S., Pagani, M., Tracy, D., Schaefer, K., Zhang, T., Pollard, D., and Beerling, D. J.: Past extreme warming events linked to massive carbon release from thawing permafrost, Nature, 484, 87–91, 2012.

D'haenens, S., Bornemann, A., Stassen, P., and Speijer, R.: Multiple early Eocene benthic foraminiferal assemblage and δ^{13}C fluctuations at DSDP site 401 (Bay of Biscay-NE Atlantic), Mar. Micropaleontol., 88–89, 15–35, 2012.

Dickens, G. R.: Down the Rabbit Hole: toward appropriate discussion of methane release from gas hydrate systems during the Paleocene–Eocene thermal maximum and other past hyperthermal events, Clim. Past, 7, 831–846, doi:10.5194/cp-7-831-2011, 2011.

Dickens, G. R., Castillo, M. M., and Walker, J. C. G.: A blast of gas in the latest Paleocene: simulating first-order effects of massive dissociation of oceanic methane hydrate, Geology, 25, 259–262, 1997.

Dickson, A. J., Rees-Owen, R. L., März, C., Coe, A. L., Cohen, A. S., Pancost, R. D., Taylor, K., and Shcherbinina, E.: The spread of marine anoxia on the northern Tethys margin during the Paleocene–Eocene thermal maximum, Paleoceanography, 29, 471–488, doi:10.1002/2014PA002629, 2014.

Di Napoli Alliata, E., Proto Decima, F., and Pellegrini, G. B.: Studio geologico, stratigrafico e micropaleontologico dei dintorni di Belluno, Memorie della Società Geologica Italiana, 9, 1–28, 1970.

Title Page

Abstract | Introduction

Conclusions | References

Tables | Figures

|◄ | ►|

◄ | ►

Back | Close

Full Screen / Esc

Printer-friendly Version

Interactive Discussion

Dunkley Jones, T., Lunt, D. J., Schmidt, D. N., Ridgwell, A., Sluijs, A., Valdez, P. J., and Maslin, M. A.: Climate model and proxy data constraints on ocean warming across the Paleocene–Eocene Thermal Maximum, Earth-Sci. Rev., 125, 123–145, 2013.

Dypvik, H., Riber, L., Burca, F., Rüther, D., Jargvoll, D., Nagy, J., and Jochmann, M.: The Paleocene–Eocene thermal maximum (PETM) in Svalbard – clay mineral and geochemical signals, Palaeogeogr. Palaeocl., 302, 156–169, 2011.

Egger, H., Fenner, J., Heilmann-Clausen, C., Roegl, F., Sachsenhofer, R. F., and Schmitz, B.: Paleoproductivity of the northwestern Tethyan margin (Anthering section, Austria) across the Paleocene–Eocene transition, in: Causes and Consequences of Globally Warm Climates in the Early Paleogene, edited by: Wing, S. L., Gingerich, P. D., Schmitz, B., and Thomas, E., Geol. S. Am. S., Boulder, Colorado, The Geological Society of America, 369, 133–146, 2003.

Egger, H., Homayoun, M., Huber, H., Roegl, F., and Schmitz, B.: Early Eocene climatic, volcanic, and biotic events in the northwestern Tethyan Untersberg section, Austria, Palaeogeogr. Palaeocl., 217, 243–264, 2005.

Egger, H., Heilmann-Clausen, C., and Schmitz, B.: From shelf to abyss: record of the Paleocene/Eocene-boundary in the Eastern Alps (Austria), Geol. Acta, 7, 215–227, doi:10.1344/105.000000266, 2009.

Ernst, S. R., Guasti, E., Dupuis, C., and Speijer, R. P., Environmental perturbation in the southern Tethys across the Paleocene/Eocene boundary (Dababiya, Egypt): foraminiferal and clay minerals record, Mar. Micropaleontol., 60, 89–111, 2006.

Fenero, R., Thomas, E., Alegret, L., and Molina, E.: Oligocene benthic foraminifera in the Fuente Caldera section (Betic Cordillera, Spain): paleoenvironmental inferences, J. Foramin. Res., 42, 286–304, 2012.

Fontanier, C., Jorissen, F. J., Chaillou, G., Anschutz, P., Gremare, A., and Griveaud, C.: Live foraminiferal faunas from a 2800 m deep lower canyon station from the Bay of Biscay: faunal response to focusing of refractory organic matter, Deep-Sea Res. I, 52, 1189–1227, 2008.

Foreman, B. Z., Heller, P. L., and Clementz, M. T.: Fluvial response to abrupt global warming at the Palaeocene/Eocene boundary, Nature, 491, 92–95, 2014.

Fornaciari, E., Giusberti, L., Luciani, V., Tateo, F., Agnini, C., Backman, J., Oddone, M., and Rio, D.: An expanded Cretaceous–Tertiary transition in a pelagic setting of the Southern Alps (central–western Tethys), Palaeogeogr. Palaeocl., 255, 98–131, 2007.

Benthic foraminifera at the Paleocene/Eocene thermal maximum

L. Giusberti et al.

Frenzel, P.: Die benthischen Foraminiferen der Ruegener Schreibkreide (Unter Maastricht, NE Deutschland), Neue Palaeontologische Abhandlungen, Dresden, Germany, CPress Verlag, Band 3, 2000.

Friedrich, O.: Benthic foraminifera and their role to decipher paleoenvironment during mid-Cretaceous Oceanic Anoxic Events-"the anoxic benthic foraminifera" paradox, Revue de Micropaléontologie, 177, 2–18, 2009.

Friedrich, O., Nishi, H., Pross, J., Schmiedel, G., and Hemleben, C.: Millennial-to centennial scale interruptions of the Oceanic Anoxic Event 1b (early Albian, mid Cretaceous) inferred from benthic foraminiferal repopulation events, Palaios, 20, 64–77, 2005.

Galeotti, S., Bellagamba, M., Kaminski, M. A., and Montanari, A.: Deep-sea benthic foraminiferal recolonisation following a volcaniclastic event in the lower Campanian of the Scaglia Rossa Formation (Umbria-Marche Basin, central Italy), Mar. Micropaleontol., 44, 57–76, 2002.

Galeotti, S., Kaminski, M. A., Coccioni, R., and Speijer, R.: High resolution deep water agglutinated foraminiferal record across the Paleocene/Eocene transition in the Contessa Road Section (central Italy), in: Proceedings of the Sixth International Workshop on Agglutinated Foraminifera, edited by: Bubik, M. and Kaminski, M. A., Grzybowski Foundation Special Publication, Grzybowski Foundation Special Publication, Drukarnia Narodowa, Kraków, 8, 83–103, 2004.

Garel, S., Schnyder, J., Jacob, J., Dupuis, C., Boussafir, M., Le Milbeau, C., Storme, J.-Y., Iakovleva, A. I., Yans, J., Baudin, F., Fléhoc, C., and Quesnel, F.: Paleohydrological and paleoenvironmental changes recorded in terrestrial sediments of the Paleocene–Eocene boundary (Normandy, France), Palaeogeogr. Palaeocl., 376, 184–199, 2013.

Gibbs, S. J., Bralower, T. J., Bown, P. R., Zachos, J. C., and Bybell, L. M.: Shelf and open-ocean calcareous phytoplankton assemblages across the Paleocene–Eocene thermal maximum: implications for global productivity gradients, Geology, 34, 233–236, 2006.

Gibson, T. G., Bybell, L. M., and Owens, J. P.: Latest Paleocene lithologic and biotic events in neritic deposits of southwestern New-Jersey, Paleoceanography, 8, 495–514, 1993.

Gibson, T. G., Bybell, L. M., and Mason, D. B.: Stratigraphic and climatic implications of clay mineral changes around the Paleocene/Eocene boundary of the northeastern US margin, Sediment. Geol., 134, 65–92, 2000.

Gingerich, P. D.: Mammalian response to climate change at the Paleocene–Eocene boundary: Polecat Bench record in the northern Bighorn Basin, Wyoming, in: Causes and Conse-

quences of Globally Warm Climates in the Early Paleogene, edited by: Wing, S. L., Gingerich, P. D., Schmitz, B., and Thomas, E., Geol. S. Am. S., Boulder, Colorado, The Geological Society of America, 369, 463–478, 2003.

Giusberti, L., Rio, D., Agnini, C., Backman, J., Fornaciari, E., Tateo, F., and Oddone, M.: Mode and tempo of the Paleocene–Eocene thermal maximum from the Venetian pre-Alps, Geol. Soc. Am. Bull., 119, 391–412, 2007.

Giusberti, L., Coccioni, R., Sprovieri, M., and Tateo, F.: Perturbation at the sea floor during the Paleocene–Eocene thermal maximum: evidence from benthic foraminifera at Contessa Road, Italy, Mar. Micropaleontol., 70, 102–119, 2009.

Gooday, A. J.: Deep-sea benthic foraminiferal species which exploit phytodetritus: characteristic features and controls on distribution, Mar. Micropaleontol., 22, 187–205, 1993.

Gooday, A. J.: The biology of deep-sea Foraminifera: a review of some advances and their applications in paleoceanography, Palaios, 9, 14–31, 1994.

Gooday, A. J.: Benthic foraminifera (Protista) as tools in deep-water paleoceanography: environmental influences on faunal characteristics, Adv. Mar. Biol., 46, 1–90, 2003.

Gooday, A. J., Hughes, J. A., and Levin, L. A.: The foraminiferan macrofauna from three North Carolina (USA) slope sites with contrasting carbon flux: a comparison with the metazoan macrofauna, Deep-Sea Res. I, 48, 1709–1739, 2001.

Gooday, A. J., Nomaki, H., and Kitazato, H.: Modern deep-sea benthic foraminifera: a brief review of their morphology-based biodiversity and trophic diversity, in: Biogeochemical Controls on Palaeoceanographic Environmental Proxies, edited by: Austin, W. E. N. and James, R. H., Geol. Soc. Spec. Publ., Bath, UK, The Geological Society Publishing House, 303, 97–119, 2008.

Gupta, A. K. and Thomas, E.: Latest Miocene-Pleistocene productivity and deep-sea ventilation in the northwestern Indian Ocean (Deep Sea drilling project site 219), Paleoceanography, 14, 62–73, 1999.

Gupta, A. K. and Thomas, E.: Initiation of Northern Hemisphere glaciation and strengthening of the northeast Indian monsoon: ocean drilling program site 758, eastern equatorial Indian Ocean, Geology, 31, 47–50, 2003.

Gupta, A. K., Sundar Raj, M., Mohan, K., and De, S.: A major change in monsoon-driven productivity in the tropical Indian Ocean during ca 1.2–0.9 Myr: foraminiferal faunal and stable isotope data, Palaeogeogr. Palaeocl., 261, 234–245, 2008.

Benthic foraminifera at the Paleocene/Eocene thermal maximum

L. Giusberti et al.

Title Page

Abstract	Introduction
Conclusions	References
Tables	Figures

|◄ | ►|

◄ | ►

Back | Close

Full Screen / Esc

Printer-friendly Version

Interactive Discussion

Hammer, Ø., Harper, D. A. T., and Ryan, P. D.: PAST: paleontological statistics software package for education and data analysis, Palaeontol. Electron., 4, 1–9, 2001.

Hancock, H. J. L. and Dickens, G. R.: Carbonate dissolution episodes in Paleocene and Eocene sediment, Shatsky Rise, west-central Pacific, in: Proceedings of the Ocean Drilling Program, edited by: Bralower, T. J., Premoli Silva, I., and Malone, M. J., Scientific Results, College Station, TX (Ocean Drilling Program), 1–24, doi:10.2973/odp.proc.sr.198.116, 2005. 2005.

Handley, L., Pearson, P. N., McMillan, I. K., and Pancost, R. D.: Large terrestrial and marine carbon and hydrogen isotope excursions in a new Paleocene/Eocene boundary section from Tanzania, Earth Planet. Sc. Lett., 275, 17–25, 2008.

Handley, L., O'Halloran, A., Pearson, P. N., Hawkins, E., Nicholas, C. J., Schouten, S., McMillan, I. K., and Pancost, R. D.: Changes in the hydrological cycle in tropical East Africa during the Paleocene–Eocene thermal maximum, Palaeogeogr. Palaeocl., 329–330, 10–21, 2012.

Harding, I. C., Charles, A. J., Marshall, J. E. A., Pälike, H., Roberts, A. P., Wilson, P. A., Jarvis, E., Thorne, R., Morris, E., Moremon, R., Pearce, R. B., and Akbari, S.: Sea-level and salinity fluctuations during the Paleocene–Eocene thermal maximum in Arctic Spitsbergen, Earth Planet. Sc. Lett., 303, 97–107, 2011.

Harries, P. J. and Kauffman, E. G.: Patterns of survival and recovery following the Cenomanian-Turonian (Late Cretaceous) mass extinction in the Western Interior Basin, United States, in: Extinction Events in Earth History, edited by: Kauffman, E. G. and Walliser, O. H., Lect. Notes Earth Sci.Heidelberg, Germany, Springer-Verlag, 30, 277–298, 1990.

Harries, P. J., Kauffman, E. G., and Hansen, T. A.: Models for biotic survival following mass extinction, in: Biotic Recovery from Mass Extinction Events, edited by: Hart, M. B., Geol. Soc. Spec. Publ., The Geological Society Publishing House, Bath, UK, 120, 41–60, 1996.

Hayward, B. W., Johnson, K., Sabaa, A. T., Kawagata, S., and Thomas, E.: Cenozoic record of elongate, cylindrical, deep-sea benthic foraminifera in the North Atlantic and equatorial Pacific Oceans, Mar. Micropaleontol., 62, 141–162, 2010a.

Hayward, B. W., Sabaa, A. T., Thomas, E., Kawagata, S., Nomura, R., Schroder Adams, C., Gupta, A. K., and Johnson, K.: Cenozoic record of elongate, cylindrical, deep-sea benthic foraminifera in the Indian Ocean (ODP sites 722, 738, 744, 758, and 763), J. Foramin. Res., 40, 113–133, 2010b.

Hess, S. and Jorissen, F. J.: Distribution patterns of living benthic foraminifera from Cap Breton canyon, Bay of Biscay: faunal response to sediment instability, Deep-Sea Res. Pt. I, 56, 1555–1578, doi:10.1016/j.dsr.2009.04.003, 2009.

Benthic foraminifera at the Paleocene/Eocene thermal maximum

L. Giusberti et al.

Holbourn, A. and Kuhnt, W.: No extinctions during Oceanic Anoxic Event Ib: the Aptian-Albian benthic foraminiferal record of ODP Leg 171, in: Western North Atlantic Palaeogene and Cretaceous Palaeoceanography, edited by: Kroon, D., Norris, R. D., and Klaus, A., Geol. Soc. London, Spec. Publ. Bath, UK, The Geological Society Publishing House, 183, 73–92, 2001.

Holbourn, A., Kuhnt, W., and Erbacher, J.: Benthic foraminifers from lower Albian black shales (Site 1049, ODP Leg 171): evidence for a non "uniformitarian" record, J. Foramin. Res., 31, 60–74, 2001.

Hönisch, B., Ridgwell, A., Schmidt, D. N., Thomas, E., Gibbs, S. J., Sluijs, A., Zeebe, R., Kump, L., Martindale, R. C., Greene, S. E., Kiessling, W., Ries, J., Zachos, J. C., Royer, D. L., Barker, S., Marchitto, T. M., Moyer, R., Pelejero, C., Ziveri, P., Foster, G. L., and Williams, B.: The geological record of ocean acidification, Science, 335, 1058–1963, 2012.

Ishman, S. E. and Domack, E. W.: Oceanographic controls on benthic foraminifers from the Bellingshausen margin of the Antarctic Peninsula, Mar. Micropaleontol., 24, 119–155, 2004.

Itambi, A. C., von Dobeneck, T., Mulitza, S., Bickert, T., and Heslop, D.: Millennial-scale northwest African droughts related to Heinrich events and Dansgaard-Oeschger cycles: evidence in marine sediments from offshore Senegal, Paleoceanography, 24, PA1205, doi:10.1029/2007PA001570, 2009.

Jaramillo, C. A., Ochoa, D., Contreras, L., Pagani, M., Carvajal-Ortiz, H., Pratt, L. M., Krishnan, S., Cardona, A., Romero, M., Quiroz, L., Rodriguez, G., Rueda, M. J., De la Parra, F., Morón, S., Green, W., Bayona, G., Montes, C., Quintero, O., Ramirez, R., Mora, G., Schouten, S., Bermudez, H., Navarrete, R., Parra, F., Alvarán, M., Osorno, J., Crowley, J. L., Valencia, V., and Vervoort, J.: Effects of rapid global warming at the Paleocene–Eocene boundary on Neotropical vegetation, Science, 330, 957–961, 2010.

John, C. M., Bohaty, S. M., Zachos, J. C., Sluijs, A., Gibbs, S., Brinkhuis, H., and Bralower, T. J.: North American continental margin records of the Paleocene–Eocene thermal maximum: implications for global carbon and hydrological cycling, Paleoceanography, 23, PA2217, doi:10.1029/2007PA001465, 2008.

John, C. M., Banerjee, N. R., Longstaffe, F. J., Sica, C., Law, K. R., and Zachos, J. C.: Clay assemblage and oxygen isotopic constraints on the weathering response to the Paleocene–Eocene thermal maximum, east coast of North America, Geology, 40, 591–594, 2012.

Benthic foraminifera at the Paleocene/Eocene thermal maximum

L. Giusberti et al.

John, E. H., Pearson, P. N., Coxall, H. K., Birch, H., Wade, B. S., and Foster, G. L.: Warm ocean processes and carbon cycling in the Eocene, Philos. T. Roy. Soc. A, 371, 20130099, doi:10.1098/rsta.2013.0099, 2013.

John, E. H., Wilson, J. D., Pearson, P. N., and Ridgwell, A.: Temperature-dependent remineralization and carbon cycling in the warm Eocene oceans, Palaeogeogr. Palaeocl., 413, 158–166, 2014.

Jones, B. and Manning, D. A. C.: Comparison of geochemical indices used for the interpretation of palaeoredox conditions in ancient mudstones, Chem. Geol., 111, 111–194, doi:10.1016/0009-2541(94)90085-X, 1994.

Jones, R. W. and Charnock, M. A.: "Morphogroups" of agglutinated foraminifera, their life positions and feeding habits and potential applicability in (paleo)ecological studies, Revue de Paléobiologie, 4, 311–320, 1985.

Jorissen, F. J.: Benthic foraminiferal successions across late Quaternary Mediterranean sapropels, 153, 91–101, 1999.

Jorissen, F. J., Fontanier, C., and Thomas, E.: Paleoceanographical proxies based on deep-sea benthic foraminiferal assemblage characteristics, in: Proxies in Late Cenozoic Paleoceanography: Pt. 2: Biological tracers and biomarkers, edited by: Hillaire-Marcel, C. and A. de Vernal, A., 1, Elsevier, Amsterdam, The Netherlands, 264–325, 2007.

Kaiho, K.: Phylogeny of deep-sea calcareous trochospiral benthic foraminifera: evolution and diversification, Micropalentology, 44, 291–311, 1998.

Kaiho, K., Arinobu, T., Ishiwatari, R., Morgans, H. E. G., Okada, H., Takeda, N., Tazaki, K., Zhou, G. P., Kajiwara, Y., Matsumoto, R., Hirai, A., Niitsuma, N., and Wada, H.: Latest Paleocene benthic foraminiferal extinction and environmental changes at Tawanui, New Zealand, Paleoceanography, 11, 447–465, 1996.

Kaminski, M. A. and Gradstein, F. M.: An Atlas of Paleogene Cosmopolitan Deep-Water Agglutinated Foraminifera, Grzybowski Foundation Special Publication, Drukarnia Narodowa, Kraków,, 10, 547 pp., 2005.

Kaminski, M. A., Kuhnt, W., and Radley, J. D.: Paleocene–Eocene deep water agglutinated foraminifera from the Numidian Flysch (Rift, Northern Morocco): their significance for the paleoceanography of the Gibraltar gateway, J. Micropaleontol., 15, 1–19, 1996.

Katz, M. E., Wright, J. D., Katz, D. R., Miller, K. G., Pak, D. K., Shackleton, N. J., and Thomas, E.: Early Cenozoic benthic foraminiferal isotopes: species reliability and interspecies correction factors, Paleoceanography, 18, 1024, doi:10.1029/2002PA000798, 2003.

Benthic foraminifera at the Paleocene/Eocene thermal maximum

L. Giusberti et al.

Title Page

Abstract | Introduction

Conclusions | References

Tables | Figures

|◄ | ►|

◄ | ►

Back | Close

Full Screen / Esc

Printer-friendly Version

Interactive Discussion

Kauffman, E. G. and Harries, P. J.: The importance of crisis progenitors in recovery from mass extinction, in: Biotic Recovery from Mass Extinction Events, edited by: Hart, M. B., Geol. Soc. Spec. Publ., The Geological Society Publishing House, Bath, UK, 120, 41–60, 1996.

Kelly, D. C., Bralower, T. J., Zachos, J. C., Premoli Silva, I., and Thomas, E.: Rapid diversification of planktonic foraminifera in the tropical Pacific (ODP site 865) during the late Paleocene thermal maximum, Geology, 24, 423–426, 1996.

Kelly, D. C., Bralower, T. J., and Zachos, J. C.: Evolutionary consequences of the latest Paleocene thermal maximum for tropical planktonic foraminifera, Palaeogeogr. Palaeocl., 141, 139–161, 1998.

Kelly, D. C., Nielsen, T. M. J., Mccarren, H. K., Zachos, J. C., and Röhl, U.: Spatiotemporal patterns of carbonate sedimentation in the South Atlantic: implications for carbon cycling during the Paleocene–Eocene thermal maximum, Palaeogeogr. Palaeocl., 293, 30–40, 2010.

Kender, S., Stephenson, M. H., Riding, J., B., Leng, M. J., O'BKnox, R. W., Peck, V. L., Kendrick, C. P., Ellis, M. A., Vane, C. H., and Jamieson, R.: Marine and terrestrial environmental changes in NW Europe preceding carbon release at the Paleocene–Eocene transition, Earth Planet. Sc. Lett., 353–354, 108–120, 2012.

Kennett, J. P. and Stott, L. D.: Abrupt deep-sea warming, palaeoceanographic changes and benthic extinctions at the end of the Palaeocene, Nature, 353, 225–229, 1991.

Kirtland Turner, S. and Ridgwell, A.: Recovering the true size of an Eocene hyperthermal from the marine sedimentary record, Paleoceanography, 28, 700–712, 2013.

Koutsoukos, E. A. M., Leary, P. M., and Hart, M. B.: Latest Cenomanian–earliest Turonian low-oxygen tolerant benthonic foraminifera: a case study from the Sergipe Basin (N. E. Brazil) and the western Anglo-Paris Basin (southern England), Palaeogeogr. Palaeocl., 77, 145–177, 1990.

Kraus, M. J. and Riggins, S.: Transient drying during the Paleocene–Eocene thermal maximum (PETM): analysis of paleosols in the Bighorn Basin, Wyoming, Palaeogeogr. Palaeocl., 245, 444–461, 2007.

Kraus, M. J., McInerney, F. A., Wing, S. L., Secord, R., Baczynski, A. A., and Bloch, J. I.: Paleohydrologic response to continental warming during the Paleocene–Eocene thermal maximum, Bighorn Basin, Wyoming, Palaeogeogr. Palaeocl., 370, 196–208, 2013.

Krishnan, S., Pagani, M., and Agnini, C.: Leaf waxes as recorders of paleoclimatic changes during the Paleocene–Eocene thermal maximum: regional expressions from the Belluno Basin, Org. Geochem., 80, 8–17, 2015.

Benthic foraminifera at the Paleocene/Eocene thermal maximum

L. Giusberti et al.

Kuhnt, W.: Abyssal recolonization by benthic foraminifera after the Cenomanian/Turonian boundary anoxic event in the North Atlantic, Mar. Micropaleontol., 19, 257–274, 1992.

Kuhnt, W.: Early Danian benthic foraminiferal community structures, Geulhmmerberg, SE Netherlands, Geol. Mijnbouw., 75, 163–172, 1996.

Kuhnt, W. and Kaminski, M. A.: Changes in the community structure of deep-water agglutinated foraminifers across the K/T boundary in the Basque Basin (northern Spain), Revista Española de Micropaleontologia, 25, 57–92, 1993.

Kuhnt, W. and Kaminski, M. A.: The reponse of benthic foraminifera to the K/T boundary event- a review, in: Géologie de l'Afrique et de l'Atlantique Sud-Comptes Rendu des Colloques de géologie d'Angers, 16–20 Juillet, 1994, edited by: Jardiné, S., de Klasz, I., and Debenay, J. P., B. Cent. Rech. Expl., Memoire, Pau, Société nationale Elf Aquitaine, 16, 433–442, 1996.

Kuhnt, W. and Collins, E. S.: Cretaceous to Paleogene benthic foraminifers from the Iberia abyssal plain, in: Proceedings of the ODP, edited by: Whitmarsh, R. B., Sawyer, D. S., Klaus, A., and Masson, D. G., Scientific Results, 149, College Station, TX Ocean Drilling Program, 203–316, 1996.

Kuhnt, W., Collins, E., and Scott, D. B.: Deep water agglutinated foraminiferal assemblages across the Gulf Stream: distribution pattern and taphonomy, in: Proceedings of the Fifth International Workshop on Agglutinated Foraminifera, edited by: Hart, M. B., Kaminski, M. A., and Smart, C. W., Grzybowski Foundation Special Publication, Drukarnia Narodowa, Kraków,, 7, 261–298, 2000.

Larrasoaña, J. C., Roberts, A. P., Rohling, E. J., Winklhofer, M., and Wehausen, R.: Three million years of monsoon variability over the northern Sahara, Clim. Dynam., 21, 689–698, doi:10.1007/s00382-003-0355-z, 2003.

Lirer, F.: A new technique for retrieving calcareous microfossils from lithified lime deposits, Micropaleontology, 46, 365–369, 2000.

Littler, K., Röhl, U., Westerhold, T., and Zachos, J. C.: A high-resolution benthic stable-isotope record for the South Atlantic: implications for orbital-scale changes in Late Paleocene–Early Eocene climate and carbon cycling, Palaeogeogr. Palaeocl., 401, 18–30, 2014.

Luciani, V., Giusberti, L., Agnini, C., Backman, J., Fornaciari, E., and Rio, D.: The Paleocene–Eocene thermal maximum as recorded by Tethyan planktonic foraminifera in the Forada section (northern Italy), Mar. Micropaleontol., 64, 189–214, 2007.

Benthic foraminifera at the Paleocene/Eocene thermal maximum

L. Giusberti et al.

Title Page

Abstract	Introduction
Conclusions	References
Tables	Figures

◀◀ ▶▶

◀ ▶

Back Close

Full Screen / Esc

Printer-friendly Version

Interactive Discussion

Ly, A. and Kuhnt, W.: Late Cretaceous benthic foraminiferal assemblages of the Casamance Shelf (Senegal, NW Africa) indication of a Late Cretaceous oxygen minimum zone, Revue de Micropaléontologie, 37, 49–74, 1994.

Ma, Z., Gray, E., Thomas, E., Murphy, B., Zachos, J. C., and Paytan, A.: Carbon sequestration during the Paleocene–Eocene thermal maximum by an efficient biological pump, Nat. Geosci., 7, 382–388, 2014.

Mancin, N., Hayward, B. W., Trattenero, I., Cobianchi, M., and Lupi, C.: Can the morphology of deep-sea benthic foraminifera reveal what caused their extinction during the mid-Pleistocene Climate Transition?, Mar. Micropaleontol., 104, 53–70, 2013.

McCarren, H., Thomas, E., Hasegawa, T., Röhl, U., and Zachos, J. C.: Depth dependency of the Paleocene–Eocene carbon isotope excursion: paired benthic and terrestrial biomarker records (ODP leg 208, Walvis Ridge), Geochem. Geophy. Geosy., 9, Q10008, doi:10.1029/2008GC002116, 2008.

McInerney, F. A. and Wing, S. L.: The Paleocene–Eocene thermal maximum: a perturbation of carbon cycle, climate, and biosphere with implications for the future, Annu. Rev. Earth Pl. Sc., 39, 489–516, doi:10.1146/annurev-earth-040610-133431, 2011.

Meissner, K. J., Bralower, T. J., Alexander, K., Dunkley Jones, T., Sijp. W., and Ward, M.: The Paleocene–Eocene Thermal Maximum: how much carbon is enough?, Paleoceanography, 29, 946–963, 2014.

Mohan, K., Gupta, A. K., and Bhaumik, A. K.: Distribution of deep-sea benthic foraminifera in the Neogene of Blake Ridge, NW Atlantic Ocean, J. Micropalaeontol., 30, 33–74, 2011.

Murphy, B. H., Farley, K. A., and Zachos, J. C.: An extraterrestrial 3He-based timescale for the Paleocene–Eocene thermal maximum (PETM) from Walvis Ridge, IODP Site 1266, Geochim. Cosmochim. Ac., 74, 5098–5108, 2010.

Murray, J. W.: Ecology and Palaeoecology of Benthic Foraminifera Longman, Harlow, 397 pp., 1991.

Murray, J. W.: Ecology and Applications of Benthic Foraminifera, Cambridge University Press, USA, 426 pp., 2006.

Murray, J. W. and Pudsey, C. J.: Living (stained) and dead foraminifra from the newly ice-free Larsen Ice Shelf, Weddell Sea, Antarctica: ecology and taphonomy, Mar. Micropaleontol., 53, 67–81, 2004.

Benthic foraminifera at the Paleocene/Eocene thermal maximum

L. Giusberti et al.

Nicolo, M. J., Dickens, G. R., and Hollis, C. J., South Pacific intermediate water oxygen depletion at the onset of the Paleocene–Eocene thermal maximum as depicted in New Zealand margin sections, Paleoceanography, 25, PA4210, doi:10.1029/2009PA001904, 2010.

Nomura, R.: Paleogene to Neogene deep-sea paleoceanography in the eastern Indian Ocean: benthic foraminifera from ODP Sites 747, 757 and 758, Micropaleontology, 41, 251–290, 1995.

Ortiz, N.: Differential patterns of benthic foraminiferal extinctions near the Paleogene/Eocene boundary in the North Atlantic and western Tethys, Mar. Micropaleontol., 26, 341–359, 1995.

Ortiz, S., Alegret, L., Payros, A., Orue-Extebarria, X., Apellaniz, E., and Molina, E.: Distribution pattern of benthic foraminifera across Ypresian-Lutetian Gorrondatxe section, Northern Spain: response to sedimentay disturbance, Mar. Micropaleontol., 78, 1–13, 2011.

Pagani, M., Caldeira, K., Archer, D., and Zachos, J. C.: An ancient carbon mystery, Science, 314, 1556–1557, 2006a.

Pagani, M., Pedentchouk, N., Huber, M., Sluijs, A., Schouten, S., Brinkhuis, H., Sinninghe Damsté, J. S., Dickens, G. R., and the Expedition 302 Scientists: Arctic hydrology during global warming at the Palaeocene/Eocene thermal maximum, Nature, 442, 671–675, 2006b.

Pälike, C., Delaney, M. L., and Zachos, J. C.: Deep-sea redox across the Paleocene–Eocene thermal maximum, Geochem. Geophy. Geosy., 15, 1038–1053, 2014.

Panchuk, K., Ridgwell, A., and Kump, L. R.: Sedimentary response to Paleocene–Eocene thermal maximum carbon release: a model-data comparison, Geology, 36, 315–318, 2008.

Panieri, G. and Sen Gupta, B. K.: Benthic foraminifera of the Blake Ridge hydrate mound, Western North Atlantic Ocean, Mar. Micropaleontol., 66, 91–102, 2007.

Paytan, A., Averyt, K., Faul, K., Gray, E., and Thomas, E.: Barite accumulation, ocean productivity, and Sr/Ba in barite across the Paleocene–Eocene thermal maximum, Geology, 35, 1139–1142, 2007.

Pearson, P. N. and Thomas, E.: Drilling disturbance and constraints on the onset of the Paleocene–Eocene boundary carbon isotope excursion in New Jersey, Clim. Past, 11, 95–104, doi:10.5194/cp-11-95-2015, 2015.

Penman, D. E., Hönisch, B., Zeebe, R. E, Thomas, E., and Zachos, J. C., Rapid and sustained surface ocean acidification during the Paleocene–Eocene thermal maximum, Paleoceanography, 29, 357–369, doi:10.1002/2014PA002621, 2014.

Pflum, C. E. and Frerichs, W. E.: Gulf of Mexico deep-water foraminifers, Cushman Foundation for Foraminiferal Research, Special Publication, 14, 125 pp., 1976.

Title Page

Abstract | Introduction

Conclusions | References

Tables | Figures

◄ | ►

◄ | ►

Back | Close

Full Screen / Esc

Printer-friendly Version

Interactive Discussion

Pierrehumbert, R. T.: The hydrologic cycle in deep-time climate problems, Nature, 419, 191–198, 2002.

Post, J. E., Thomas, E., and Heaney, P. J.: Jianshuiite in oceanic manganese nodules at the Paleocene–Eocene boundary, Am. Mineral., in press, 2015.

5 Raymo, M. E., Ruddiman, F., and Froelich, P. N.: Influence of late Cenozoic mountain building on ocean geochemical cycles, Geology, 16, 649–653, 1988.

Ravizza, G. E., Norris, R. N., Blusztajn, J., and Aubry, M.-P.: An osmium isotope excursion associated with the late Paleocene thermal maximum: evidence of intensified chemical weathering, Paleoceanography, 16, 155–163, 2001.

10 Robert, C. and Chamley, H.: Development of early Eocene warm climates, as inferred from clay mineral variations in oceanic sediments, Global Planet. Change, 89, 315–331, 1991.

Robert, C. and Kennett, J. P.: Antarctic subtropical humid episode at the Paleocene–Eocene boundary: clay–mineral evidence, Geology, 22, 211–214, 1994.

Rodriguez-Tovar, F. J., Uchman, A., Alegret, L., and Molina, E.: Impact of the Paleocene–

15 Eocene thermal maximum on the macrobenthic community: ichnological record from the Zumaia section, northern Spain, Mar. Geol., 282, 178–187, 2011.

Röhl, U., Westerhold, T., Bralower, T. J., and Zachos, J. C.: On the duration of the Paleocene–Eocene thermal maximum (PETM), Geochem. Geophy. Geosy., 8, Q12002, doi:10.1029/2007GC001784, 2007.

20 Sachse, D., Radke, J., and Gleixner, G.: δD values of individual n-alkanes from terrestrial plants along a climatic gradient-implications for the sedimentary biomarker record, Org. Geochem., 37, 469–483, 2006.

Schmiedl, G.: Late Quaternary benthic foraminiferal assemblages from the eastern South Atlantic: reconstruction of deep-water circulation and productivity changes, Reports on Polar

25 Research, Bremerhaven, 160, 207 pp., (in German), 1995.

Schmiedl, G. and Mackensen, A.: Late Quaternary paleoproductivity and deep water circulation in the eastern South Atlantic Ocean: evidence from benthic foraminifera, Palaeogeogr. Palaeocl., 130, 43–80, 1997.

Schmiedl, G., De Bovee, F., Buscail, R., Charriere, B., Hemleben, C., Medernach, L., and Pi-

30 con, P.: Trophic control of benthic foraminiferal abundance and microhabitat in the bathyal Gulf of Lions, western Mediterranean Sea, Mar. Micropaleontol., 40, 167–188, 2000.

Title Page

Abstract | Introduction

Conclusions | References

Tables | Figures

|◀ | ▶|

◀ | ▶

Back | Close

Full Screen / Esc

Printer-friendly Version

Interactive Discussion

Schmitz, B. and Pujalte, V.: Sea-level, humidity, and land-erosion records across the initial Eocene thermal maximum from a continental-marine transect in northern Spain, Geology, 31, 689–692, 2003.

Schmitz, B. and Pujalte, V.: Abrupt increase in seasonal extreme precipitation at the Paleocene–Eocene boundary, Geology, 35, 215–218, 2007.

Schmitz, B., Pujalte, V., and Nùñez-Betelu, K.: Climate and sea level perturbations during the initial Eocene thermal maximum: evidence from siliciclastic units in the Basque Basin (Ermua, Zumaia and Trabakua Pass), northern Spain, Palaeogeogr. Palaeocl., 165, 299–320, 2001.

Schmitz, B., Asaro, F., Molina, E., Monechi, S., Von Salis, K., and Speijer, R.: High resolution iridium, δ^{13}C, δ^{18}O, foraminifera and nannofossil profiles across the latest Paleocene benthic extinction event at Zumaya, Palaeogeogr. Palaeocl., 133, 49–68, 1997.

Schoon, P. L., Heilmann-Clausen, C., Schultz, B. P., Sinninghe Damsté, J. S., and Schouten, S.: Warming and environmental changes in the eastern North Sea Basin during the Palaeocene–Eocene thermal maximum as revealed by biomarker lipids, Org. Geochem., 78, 79–88, 2015.

Secord, R., Gingerich, P. D., Lohmann, K. C., and MacLeod, K. G., Continental warming preceding the Palaeocene–Eocene thermal maximum, Nature, 467, 955–958, 2010.

Sgarrella, F., Sprovieri, F., Di Stefano, E., and Caruso, S.: Paleoceanography conditions at the base of the Pliocene in the Southern Mediterranean Basin, Riv. Ital. Paleontol. S., 103, 207–220, 1997.

Sing, R. K. and Gupta, A. K.: Late Oligocene–Miocene paleoceanographic evolution of the southeastern Indian Ocean: evidence from deep-sea benthic foraminifera (ODP Site 757), Mar. Micropaleontol., 51, 153–170, 2004.

Sluijs, A. and Brinkhuis, H.: A dynamic climate and ecosystem state during the Paleocene–Eocene Thermal Maximum: inferences from dinoflagellate cyst assemblages on the New Jersey Shelf, Biogeosciences, 6, 1755–1781, doi:10.5194/bg-6-1755-2009, 2009.

Sluijs, A., Schouten, S., Pagani, M., Woltering, M., Brinkhuis, H., Sinninghe Damsté, J. S., Dickens, G. R., Huber, M., Reichart, G. J., and Stein, R.: Subtropical Arctic Ocean temperatures during the Palaeocene/Eocene thermal maximum, Nature, 441, 610–613, 2006.

Sluijs, A., Bowen, G. J., Brinkhuis, H., Lourens, L. J., and Thomas, E.: The Paleocene–Eocene thermal maximum super greenhouse: biotic and geochemical signatures, age models and mechanisms of global change, in: Deep-Time Perspectives on Climate Change: marrying

Benthic foraminifera at the Paleocene/Eocene thermal maximum

L. Giusberti et al.

the Signal From Computer Models and Biological Proxies, edited by: Williams, M., Haywood, A.M., Gregory, F. J., and Schmidt, D. N., The Micropalaeontological Society Special Publication, The Geological Society, London, 323–350, 2007a.

Sluijs, A., Brinkhuis, H., Schouten, S., Bohaty, S. M., John, C. M., Zachos, J. C., Reichart, G.-J., Sinninghe Damsté, J. S., Crouch, E. M., and Dickens, G. R.: Environmental precursors to rapid light carbon injection at the Palaeocene/Eocene boundary, Nature, 450, 1218–1221, 2007b.

Sluijs, A., Brinkhuis, H., Crouch, E. M., John, C. M., Handley, L., Munsterman, D., Bohaty, S. M., Zachos, J. C., Reichart, G., Schouten, S., Pancost, R. D., Sinninghe Damste, J. S., Welters, N. L. D., Lotter, A. F., and Dickens, G. R.: Eustatic variations during the Paleocene–Eocene greenhouse world, Paleoceanography, 23, PA4216, doi:10.1029/2008PA001615, 2008.

Sluijs, A., Bijl, P. K., Schouten, S., Röhl, U., Reichart, G.-J., and Brinkhuis, H.: Southern Ocean warming, sea level and hydrological change during the Paleocene–Eocene thermal maximum, Clim. Past, 7, 47–61, doi:10.5194/cp-7-47-2011, 2011.

Smith, F. A. and Freeman, K. H.: Influence of physiology and climate on δD of leaf wax n-alkanes from C3 and C4 grasses, Geochim. Cosmochim. Ac., 70, 1172–1187, 2006.

Smith, F. A., Wing, S. L., and Freeman, K. H.: Magnitude of the carbon isotope excursion at the Paleocene–Eocene thermal maximum: the role of plant community change, Earth Planet. Sc. Lett., 262, 50–65, 2007.

Speijer, R. P., Schmitz, B., Aubry, M.-P., and Charisi, S. D.: The latest Paleocene benthic extinction event: punctuated turnover in outer neritic foraminiferal faunas from Gebel Aweina, Egypt, in: Paleocene/Eocene Boundary Events in Space and Time, edited by: Aubry, M.-P., and Benjamini, C. , Israel, J. Earth Sci., 44, 207–222, 1996.

Speijer, R. P. and Schmitz, B.: A benthic foraminiferal record of Paleocene sea level and trophic/redox conditions at Gebel Aweina, Egypt, Palaeogeogr. Palaeocl., 137, 79–101, 1998.

Speijer, R. P., Scheibner, C., Stassen, P., and Morsi, A.-M.: Response of marine ecosystems to deep-time global warming: a synthesis of biotic patterns across the Paleocene–Eocene thermal maximum (PETM), Austrian Journal of Earth Sciences, 105, 6–16, 2012.

Stassen, P., Thomas, E., and Speijer, R. P.: The progression of environmental changes during the onset of the Paleocene–Eocene thermal maximum (New Jersey Coastal Plain), Austrian Journal of Earth Sciences, 105/1, 169–178, 2012a.

Stassen, P., Thomas, E., and Speijer, R. P.: Integrated stratigraphy of the Paleocene–Eocene thermal maximum in the New Jersey Coastal Plain: toward understanding the effects of global warming in a shelf environment, Paleoceanography, 27, PA4210, doi:10.1029/2012PA002323, 2012b.

Stassen, P., Thomas, E., and Speijer, R. P.: Paleocene–Eocene thermal maximum environmental change in the New Jersey Coastal Plain: benthic foraminiferal biotic events, Mar. Micropaleontol., 115, 1–23, 2015.

Stoll, H. M., Shimizu, N., Archer, D. E., and Ziveri, P.: Coccolithophore productivity response to greenhouse event of the Paleocene–Eocene thermal maximum, Earth Planet. Sc. Lett., 258, 192–206, 2007.

Suhr, S. B., Pond, D. W., Gooday, A. J., and Smith, C. R.: Selective feeding by foraminifera on phytodetritus on the western Antarctic Peninsula shelf: evidence from fatty acid biomarker analysis, Mar. Ecol.-Prog. Ser., 262, 153–162, 2003.

Takata, H., Nomura, R., and Khim, B.-K.: Response to abyssal benthic foraminifera to mid-Oligocene glacial events in the eastern Equatorial Pacific Ocean (ODP leg 199), Palaeogeogr. Palaeocl., 292, 1–11, 2010.

Takeda, K. and Kaiho, K.: Faunal turnovers in central Pacific benthic foraminifera during the Paleocene–Eocene thermal maximum, Palaeogeogr. Palaeocl., 251, 175–197, 2007.

Thiry, M.: Palaeoclimatic interpretation of clay minerals in marine deposits: an outlook from the continental origin, Earth-Sci. Rev., 49, 201–221, doi:10.1016/S0012-8252(99)00054-9, 2000.

Thomas, D. J., Bralower, T. J., and Zachos, J. C.: New evidence for subtropical warming during the late Paleocene thermal maximum: stable isotopes from Deep Sea Drilling project site 527: Walvis Ridge, Paleoceanography, 14, 561–570, doi:10.1029/1999PA900031, 1999.

Thomas, D. J., Zachos, J. C., Bralower, T. J., Thomas, E., and Bohaty, S.: Warming the fuel for the fire: evidence for the thermal dissociation of methane hydrate during the Paleocene–Eocene thermal maximum, Geology, 30, 1067–1070, 2002.

Thomas, E.: Late Eocene to Recent deep-sea benthic foraminifers from the central equatorial Pacific Ocean, in: Initial Rep. Deep Sea, edited by: Mayer, L., Theyer, F., Barron, J. A., Dunn, D. A., Handyside, T., Hills, S., Jarvis, I., Nigrini, C. A., Pisias, N. C., Pujos, A., Saito, T., Stout, P., Thomas, E., Weinreich, N., and Wilkens, R. H., 85, US Government Printing Office, Washington, 655–656, 1985.

Thomas, E.: Development of Cenozoic deep-sea benthic foraminiferal faunas in Antarctic waters, Geol. Soc. Spec. Publ., 47, 283–296, 1989.

Thomas, E.: Late Cretaceous through Neogene deep-sea benthic foraminifers (Maud Rise, Weddell Sea, Antarctica), in: Proceedings of the Ocean Drilling Program, Scientific Results, edited by: Barker, P. F., Kennett, J. P., O'Connell, S., Berkowitz, S., Bryant, W. R., Burckle, L. H., Egeberg, P. K., Fiitterer, D. K., Qersonde, R. E., Qolovchenko, X., Hamilton, N., Lawver, L., Lazarus, D. B., Lonsdale, M., Mohr, B., Nagao, T., Pereira, C. P. Q., Pudsey, C. J., Robert, C. M., Schandl, E., SpiejJ, V., Stott, L. D., Thomas, E., Thompson, K. F. M., and Wise, S. W. Jr., 113, College Station, TX (Ocean Drilling Program), 571–594, 1990.

Thomas, E.: Biogeography of the late Paleocene benthic foraminiferal extinction, in: Late Paleocene-Early Eocene Climatic and Biotic Events in the Marine and Terrestrial Records, edited by: Aubry, M. P., Lucas, S., and Berggren, W., A., Columbia University Press, New York, 214–243, 1998.

Thomas, E.: Extinction and food at the seafloor: a high-resolution benthic foraminiferal record across the Initial Eocene thermal maximum, Southern Ocean site 690, in: Causes and Consequences of Globally Warm Climates in the Early Paleogene, edited by: Wing, S. L., Gingerich, P. D., Schmitz, B., and Thomas, E., Geol. S. Am. S., Boulder, Colorado, The Geological Society of America, 369, 319–332, 2003.

Thomas, E.: Cenozoic mass extinctions in the deep sea: What perturbs the largest habitat on Earth?, in: Large Ecosystem Perturbations: Causes and Consequences, edited by: Monechi, S., Coccioni, R., and Rampino, M., Geol. S. Am. S., Boulder, Colorado, The Geological Society of America, 424, 1–23, 2007.

Thomas, E. and Gooday, A. W.: Cenozoic deep-sea benthic foraminifers: tracers for changes in oceanic productivity?, Geology, 24, 355–358, 1996.

Thomas, E. and Shackleton, N. J.: The Paleocene–Eocene benthic foraminiferal extinction and stable isotopes anomalies, Geol. Soc. Spec. Publ., 101, 401–441, 1996.

Thomas, E., Zachos, J. C., and Bralower, T. J.: Deep-Sea Environments on a Warm Earth: latest Paleocene-early Eocene, in: Warm Climates in Earth History, edited by: Huber, B., MacLeod, K., and Wing, S., Cambridge University Press, Cambridge, UK, 132–160, 2000.

Tipple, B. J., Pagani, M., Krishnan, S., Dirghangi, S. S., Galeotti, S., Agnini, C., Giusberti, L., and Rio, D.: Coupled high-resolution marine and terrestrial records of carbon and hydrologic cycles variations during the Paleocene–Eocene thermal maximum (PETM), Earth Planet. Sc. Lett., 311, 82–92, 2011.

Title Page

Abstract | Introduction

Conclusions | References

Tables | Figures

◀◀ | ▶▶

◀ | ▶

Back | Close

Full Screen / Esc

Printer-friendly Version

Interactive Discussion

Tjalsma, R. C. and Lohmann, G. P.: Paleocene–Eocene bathyal and abyssal benthic foraminifera from the Atlantic Ocean, Micropaleontology Special Publication, 4, 1–90, 1983.

Torrent, J., Barro, V., and Liu, Q.: Magnetic enhancement is linked to and precedes hematite formation in aerobic soil, Geophys. Res. Lett., 33, L02401, doi:10.1029/2005GL024818, 2006.

Van Morkhoven, F. P. C. M., Berggren, W. A., and Edwards, A. S.: Cenozoic cosmopolitan deep-water benthic foraminifera, B. Cent. Rech. Expl., 11, 1–421, 1986.

Von Hillebrandt, A.: Das Paläozän und seine Foraminiferenfauna im Becken von Reichenhall und Salzburg, Bayerische Akademie der Wissenschaften, Mathematisch-Naturwissenschaftliche Klasse, Abhandlungen, neue folge, München, 108, 9–180, 1962.

Waśkowska, A.: Response of early Eocene deep-water benthic foraminifera to volcanic ash falls in the Polish Outer Carpatians: palaeoecological implications, Palaeogeogr. Palaeocl., 305, 50–64, 2011.

Wendler, I., Huber, B. T., MacLeod, K. G., and Wendler, J. E.: Stable oxygen and carbon isotope systematics of exquisitely preserved Turonian foraminifera from Tanzania – understanding isotopic signatures in fossils, Mar. Micropaleontol., 102, 1–33, 2013.

Westerhold, T., Röhl, U., Laskar, J., Raffi, I., Bowles, J., Lourens, L. J., and Zachos, J. C.: On the duration of Magnetochrons C24r and C25n, and the timing of early Eocene global warming events: implications from the ODP leg 208 Walvis Ridge depth transect, Paleoceanography, 22, PA2201, doi:10.1029/2006PA001322, 2007.

Wieczorek, R., Fantle, M. S., Kump, L. R., and Ravizza, G.: Geochemical evidence for volcanic activity prior to and enhanced terrestrial weathering during the Paleocene Eocene thermal maximum, Geochim. Cosmochim. Ac., 119, 391–410, 2013.

Wing, S. L., Harrington, G. J., Smith, F. A., Bloch, J. I., Boyer, D. M., and Freeman, K. H.: Transient floral change and rapid global warming at the Paleocene–Eocene boundary, Science, 310, 993–996, 2005.

Winguth, A. M. E., Shellito, C., Shields, C., and Winguth, C.: Climate response at the Paleocene–Eocene thermal maximum to greenhouse gas forcing – a model study with CCSM3, J. Climate, 23, 2562–2584, doi:10.1175/2009JCLI3113.1, 2010.

Winguth, A. M. E., Thomas, E., and Winguth, C.: Global decline in ocean ventilation, oxygenation, and productivity during the Paleocene–Eocene thermal maximum: implications for the benthic extinction, Geology, 40, 263–266, 2012.

Zachos, J. C., Pagani, M., Sloan, L. C., Thomas, E., and Billups. K.: Trends, rhythms, and aberrations in global climate 65 Ma to present, Science, 292, 686–693, 2001.

Benthic foraminifera at the Paleocene/Eocene thermal maximum

L. Giusberti et al.

Zachos, J. C., Schouten, S., Bohaty, S., Quattlebaum, T., Sluijs, A., Brinkhuis, H., Gibbs, S. J., and Bralower, T. J.: Extreme warming of mid latitude coastal ocean during the Paleocene–Eocene thermal maximum: inferences from TEX86 and isotope data, Geology, 34, 737–740, 2006.

5 Zachos, J. C., Röhl, U., Schellenberg, S. A., Sluijs, A., Hodell, D. A., Kelly, D. C., Thomas, E., Nicolo, M., Raffi, I., Lourens, L. J., Mccarren, H., and Kroon, D.: Rapid acidification of the ocean during the Paleocene–Eocene thermal maximum, Science, 308, 1611–1615, 2015.

Zeebe, R. E., Zachos, J. C., and Dickens, G. R.: Carbon dioxide forcing alone insufficient to explain Paleocene–Eocene thermal maximum warming, Nat. Geosci., 2, 576–580, 2009.

10 Zeebe, R. E., Dickens, G. R., Ridgwell, A., Sluijs, A., and Thomas, E.: Onset of carbon isotope excursion at the Paleocene–Eocene thermal maximum took millennia, not 13 years (Comment), P. Natl. Acad. Sci. USA, 111, E1062–E1063, doi:/10.1073/pnas.1321177111, 2014.

Zhang, Y., Ji, J., Balsam, W. L., Liu, L., and Chen, J.: High resolution hematite and goethite records from ODP 1143, South China Sea: co-evolution of monsoonal precipitation and El

15 Niño over the past 600,000 years, Earth Planet. Sc. Lett., 264, 136–150, 2007.

Zhou, X., Thomas, E., Rickaby, R. E. M., Winguth, A. M. E., and Lu, Z.: I/Ca evidence for global upper ocean deoxygenation during the Paleocene–Eocene thermal maximum (PETM), Paleoceanography, 29, 964–975, doi:10.1002/2014PA002702, 2014.
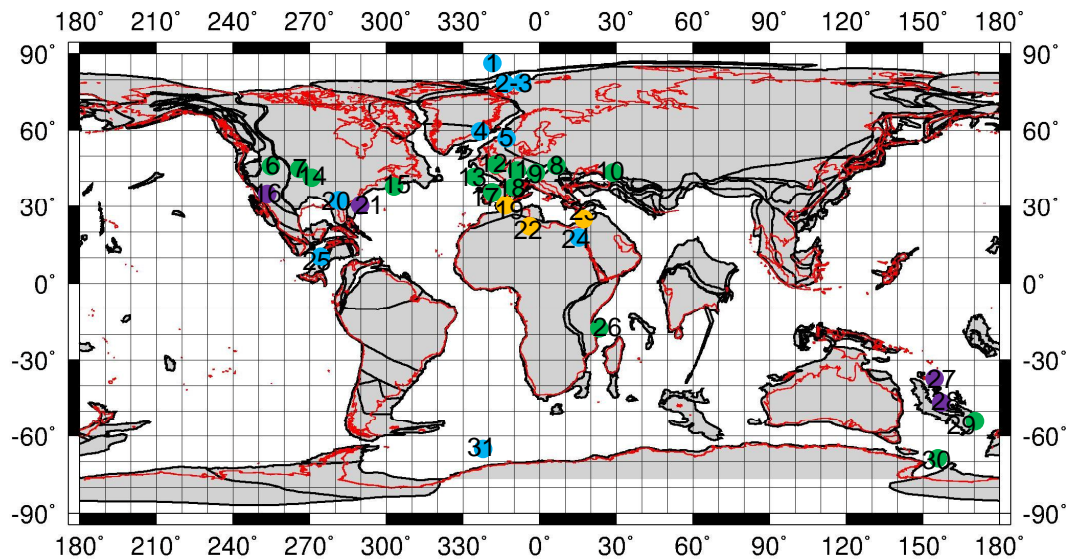
55.0 Ma Reconstruction

Figure 1. Paleogeographic map (from http://www.odsn.de/odsn/services/paleomap/paleomap.html) at 55 Ma showing sites where paleohydrological reconstructions for the PETM are available. Numbers follow a north to south paleolatitudinal order. Blue dots indicate areas where an increase in precipitation has been inferred; Green dots indicate areas where an increase in climatic contrasts or a fluctuating precipitation regime have been inferred; Orange dots indicate areas where an increase in aridity has been inferred; Purple dots indicate areas where hydrological changes have been inferred but the pattern not specified. 1. Lomonosov Ridge, Arctic sea; 2. Spitsbergen Central Basin, Iceland; 3. Svalbard archipelago; 4. Central North sea Basin; 5. Eastern North sea Basin; 6. Williston Basin, western north Dakota, (USA) 7. Bighorn Basin, Wyoming (USA); 8. Rhenodanubian Basin, Austria; 9. Belluno Basin, northeastern Italy; 10. Aktumsuk and Kaurtakapy sections, Uzbekistan and Kazakhstan; 11. Dieppe-Hampshire Basin, France; 12. London Basin; 13. DSDP Site 401 Bay of Biscay, North-Eastern Atlantic Ocean; 14. Western Colorado (USA); 15. New Jersey Coastal Plain (USA); 16. Central Valley of California (USA); 17. Basque Basin, northern Spain; 18. Tremp Basin, northern Spain; 19. Alamedilla section, southern Spain; 20. Tornillo Basin, Texas (USA); 21. Salisbury embayment, mid-Atlantic coastal plain (USA); 22. Gafsa Basin, Tunisia; 23. Zin Valley of Negev, Israel; 24. Dababya section, Egypt; 25. Northern Neotropics, (Colombia and Venezuela); 26. TDP Site 14, Tanzania; 27. Tawanui section, North Island (New Zealand); 28. Clarence River valley, South Island (New Zealand); 29. Central Westland, South Island (New Zealand); 30. ODP Site 1172, East Tasman Plateau; 31. ODP Site 690 Weddell Sea, Southern Ocean. See Supplement Table S1 for references and additional information.
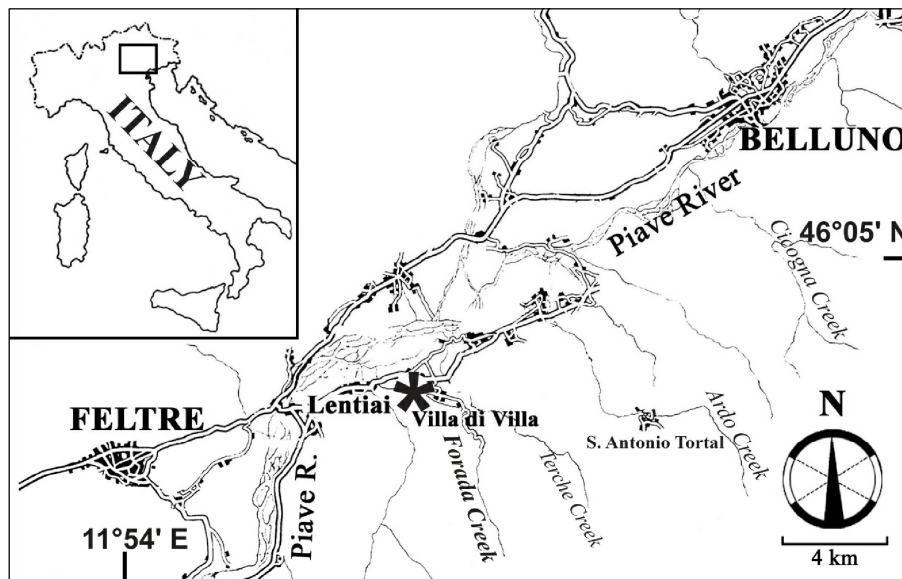
Figure 2. Location of the Forada section in the context of the Piave River Valley in the Belluno Province (the "Valbelluna"), northeastern Italy.

Discussion Paper | Discussion Paper | Discussion Paper | Discussion Paper |

CPD

11, 4205–4272, 2015

Benthic foraminifera at the Paleocene/Eocene thermal maximum

L. Giusberti et al.

Title Page

Abstract | Introduction

Conclusions | References

Tables | Figures

|◄ | ►|

◄ | ►

Back | Close

Full Screen / Esc

Printer-friendly Version

Interactive Discussion
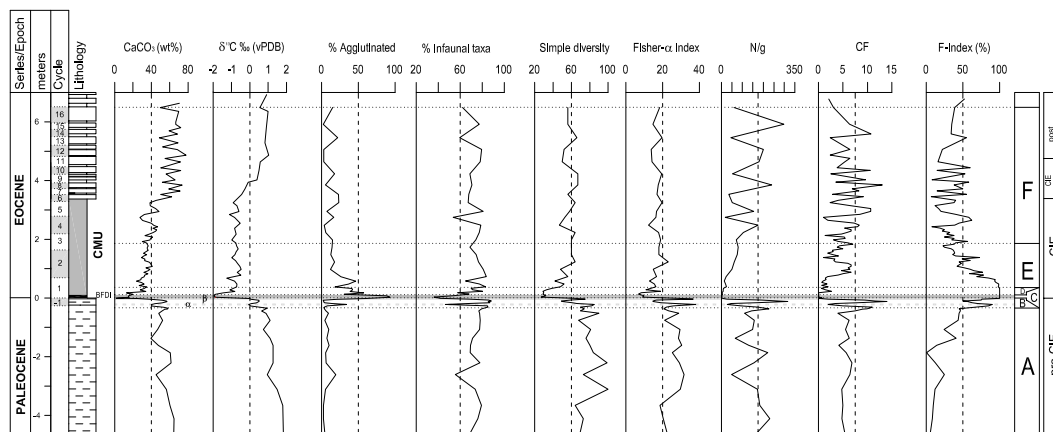
Figure 3. Faunal and geochemical variations across the PETM at Forada section plotted against chronostratigraphy, precessional cycles, lithology, recognized benthic foraminiferal assemblages (A to G) and isotopic intervals. % agglutinated = agglutinated to agglutinated and calcareous hyaline ratio; % infaunal taxa = infaunal to infaunal and epifaunal ratio; simple diversity and Fisher-α diversity index; $N\,g^{-1}$ = number of benthic foraminifera per gram (faunal density) in the > 63 mm size fraction; coarse fraction (CF) calculated according to Hancock and Dickens (2005); Fragmentation index (F Index) is from Luciani et al. (2010). The gray bands indicate intervals of carbonate dissolution. α = pre-CIE dissolution, β = burndown layer, BFDI = benthic foraminiferal dissolution interval. Modified from Giusberti et al. (2007).
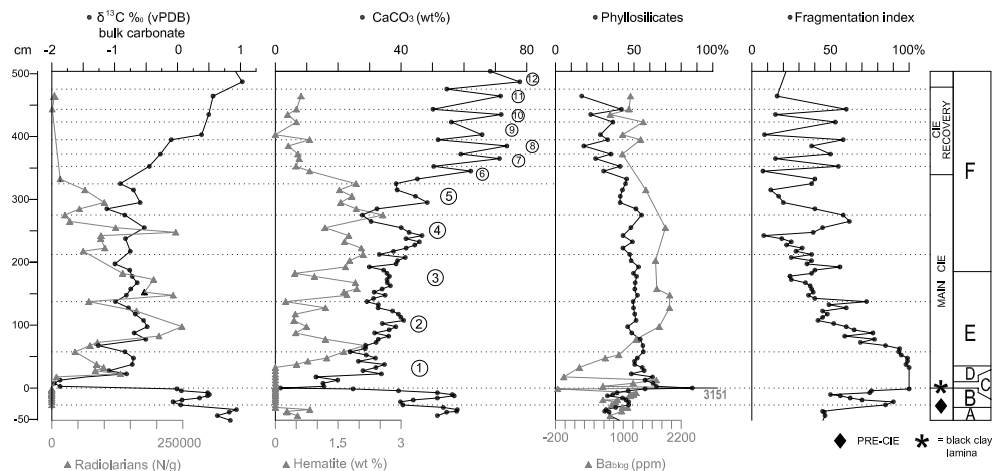
Figure 4. Summary of the main mineralogical, geochemical and cyclostratigraphic features recognized across the Paleocene–Eocene boundary and in the clay marl unit (CMU) of the Forada section and radiolarian abundance plotted against isotopic intervals and recognized benthic foraminiferal assemblages (A to F). Analyses of radiolarians are based on the fraction $> 125\,\mu m$. F Index from Luciani et al. (2010). VPDB – Vienna Peedee belemnite standard. Modified from Giusberti et al. (2007).
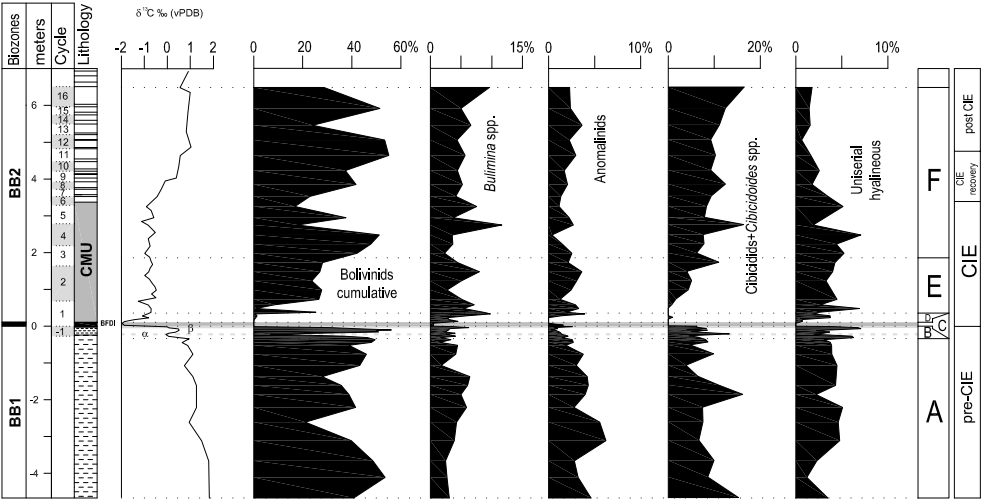
Figure 5. Relative abundance of the most abundant benthic foraminiferal taxa across the PETM at Forada plotted against biostratigraphy, precessional cycles, lithology, δ^{13}C bulk record, recognized benthic foraminiferal assemblages (A to F) and isotopic intervals. Benthic foraminiferal biozonation after Berggren and Miller (1989). The gray bands indicate intervals of carbonate dissolution. α = pre-CIE dissolution, β = burndown layer, BFDI = benthic foraminiferal dissolution interval. *Bulimina* spp. includes representative of the genus *Bulimina* and related genera as *Buliminella*, *Quadratobuliminella*, *Sitella*, *Turrilina*, etc.
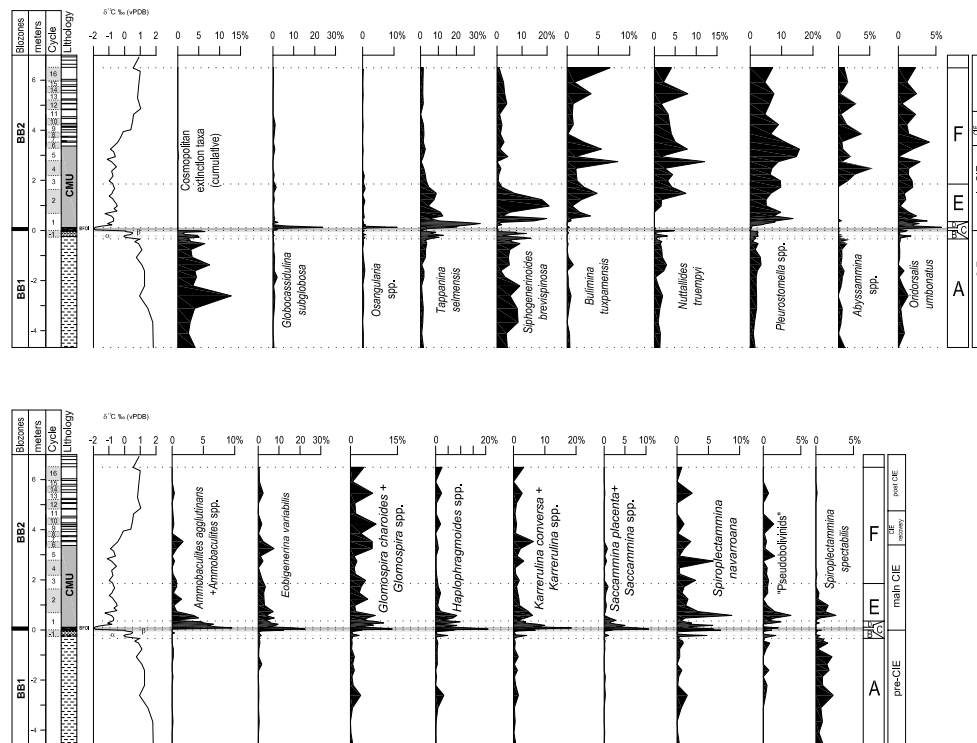
Figure 6. Relative abundance of selected benthic foraminifera across the PETM at Forada plotted against biostratigraphy, precessional cycles, lithology, δ^{13}C bulk record, recognized benthic foraminiferal assemblages (A to F) and isotopic intervals. Benthic foraminiferal biozonation after Berggren and Miller (1989). The gray bands indicate intervals of carbonate dissolution. α = pre-CIE dissolution, β = burndown layer, BFDI = benthic foraminiferal dissolution interval.

Title Page

Abstract | Introduction

Conclusions | References

Tables | Figures

|◄ | ►|

◄ | ►

Back | Close

Full Screen / Esc

Printer-friendly Version

Interactive Discussion
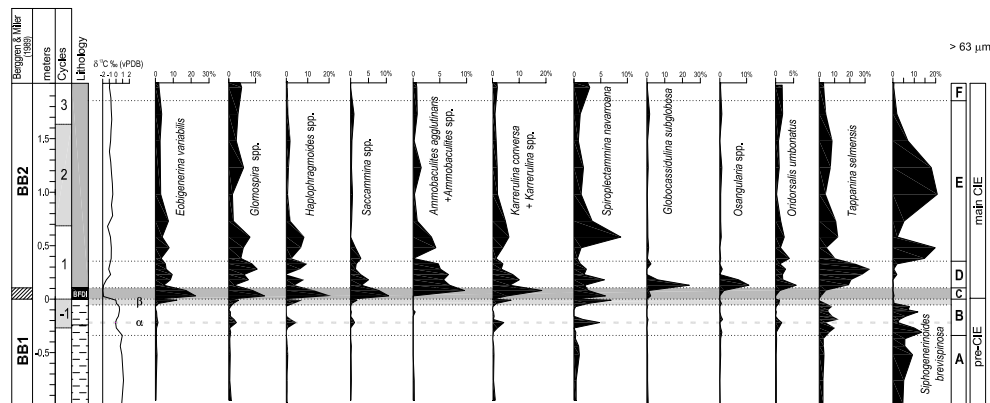
Figure 7. Enlargement of the interval from −1 m to +2 m across the P/E boundary at Forada showing the relative abundance of selected benthic foraminifera plotted against biostratigraphy, precessional cycles, lithology, δ^{13}C bulk record, recognized benthic foraminiferal assemblages (A to F) and isotopic intervals. Benthic foraminiferal biozonation after Berggren and Miller (1989). The gray bands indicate intervals of carbonate dissolution. α = Pre-CIE dissolution interval; β = burndown layer, BFDI = benthic foraminiferal dissolution interval.
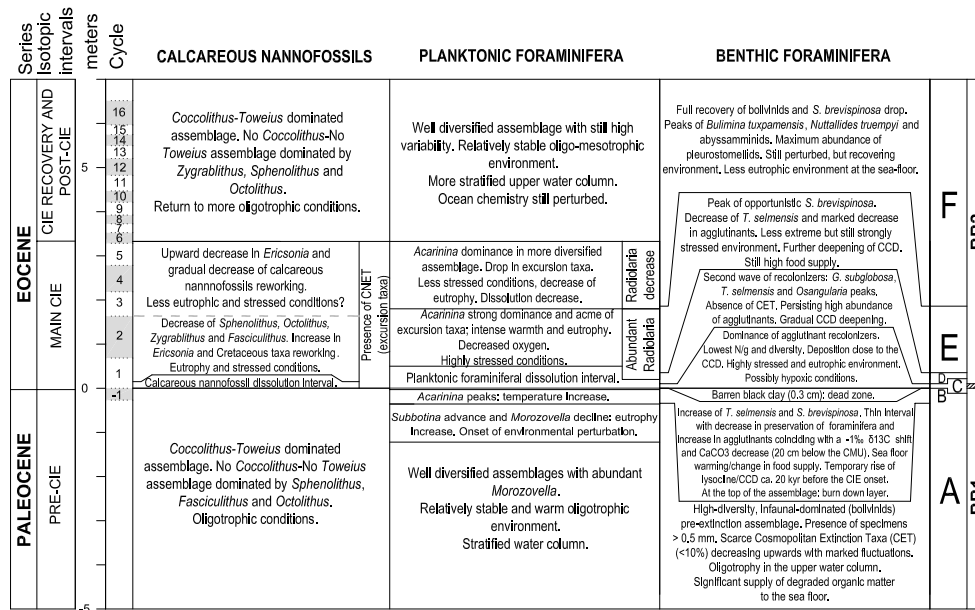
Figure 8. Summary of main calcareous plankton (calcareous nannofossils and planktonic foraminifera) and benthic foraminiferal events and inferred environmental conditions (from Agnini et al., 2007; Luciani et al., 2007 and present work), isotopic intervals, thickness, precessional cycles and benthic foraminiferal assemblages (A to F) recognized in this work. The stratigraphic intervals containing assemblages A and B, C and D to F are considered as pre-extinction, extinction and repopulation intervals, respectively. Benthic foraminiferal zonation after Berggren and Miller (1989).
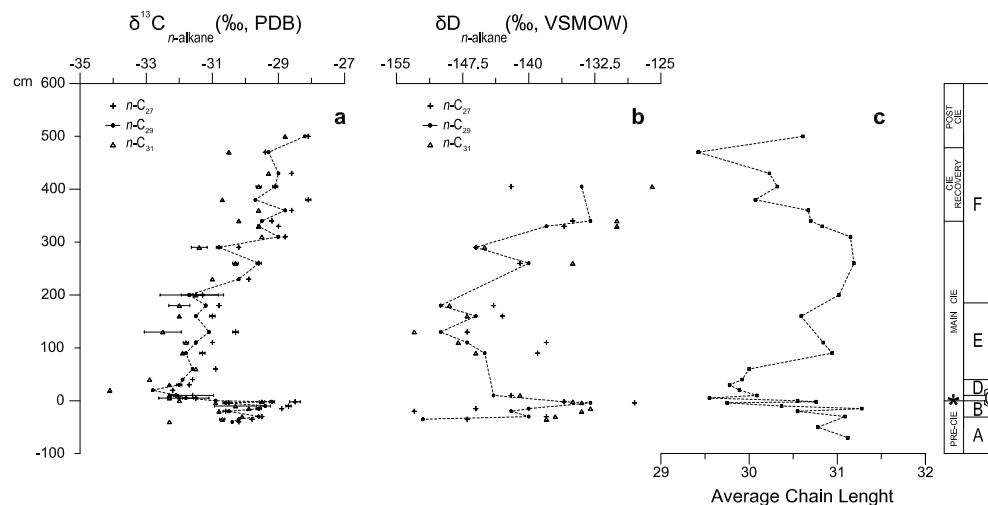
Figure 9. Stable carbon isotope ratios of higher plant *n*-alkanes **(a)**, stable hydrogen isotope ratios of higher plant *n*-alkanes **(b)** with higher plant average chain length values **(c)** for Forada PETM plotted against isotopic intervals and recognized benthic foraminiferal assemblages (A to F). Terrestrial higher plant n-C27, n-C29, and n-C31 δD values are shown as crosses, closed circles, and triangles, respectively. Redrawn from data of Tipple et al. (2011).
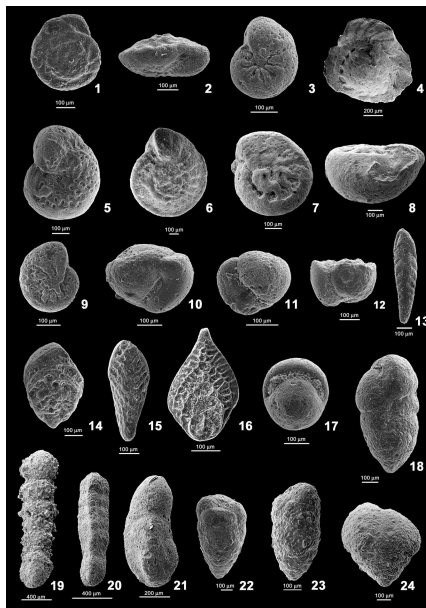
Plate 1. SEM micrographs of the most representative Paleocene cosmopolitan extinction taxa (CET) occurring at Forada. 1. *Angulogavelinella avnimelechi*, spiral view (BRI −25.5); 2. *Angulogavelinella avnimelechi*, lateral view (BRI −185.5); 3. *Gavelinella beccariiformis*, umbilical view (BRI −75); 4. *Osangularia velascoensis*, spiral view (BRI −50,5); 5. *Anomalinoides rubiginosus* (BRI −9); 6. *Cibicidoides dayi* (BRI −37); 7. *Cibicidoides velascoensis*, spiral view (BRI −75,5); 8. *Cibicidoides velascoensis*, lateral view (BRI −135.5); 9. *Cibicidoides hyphalus* (BRI −50,5); 10. ”*Neoeponides*” *megastoma* (BRI −135); 11. *Gyroidinoides globosus* (BRI −50.5); 12. *Gyroidinoides quadratus* (BRI −185,5); 13. *Coryphostoma midwayensis* (BRI −50,5); 14. *Aragonia velascoensis* (BRI −50.5); 15. *Bolivinoides delicatulus* (BRI −135.5); 16. *Neoflabellina semireticulata* (BRI −365); 17. *Pullenia coryelli* (BRI −50,5); 18. *Remesella varians* (BRI −310.5); 19. *Clavulinoides globulifera* (BRI −25.5); 20. *Clavulinoides trilatera* (BRI −33); 21. *Clavulinoides amorpha*; 22. *Marssonella indentata* (BRI −25.5); 23. *Dorothia beloides* (BRI −260); 24. *Dorothia pupa* (BRI −105).

Title Page

Abstract | Introduction

Conclusions | References

Tables | Figures

◄◄ | ►►

◄ | ►

Back | Close

Full Screen / Esc

Printer-friendly Version

Interactive Discussion

Title Page

Abstract | Introduction

Conclusions | References
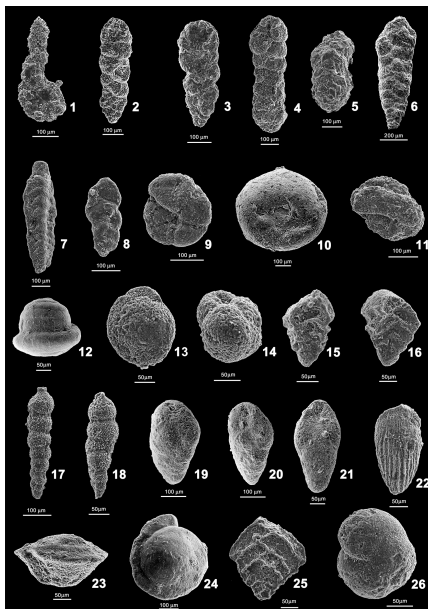
Tables | Figures

|◄ | ►|

◄ | ►

Back | Close

Full Screen / Esc

Printer-friendly Version

Interactive Discussion

Plate 2. SEM micrographs of the most representative species of the Eocene postextinction faunas occurring at Forada. 1. *Ammobaculites agglutinans* (BRI +10); 2. *Eobigenerina variabilis* (BRI +50); 3. *Eobigenerina variabilis* (BRI +50); 4. *Karrerulina conversa* (BRI +50); 5. *Karrerulina horrida* (BRI −25.5); 6. *Spiroplectammina navarroana* (BRI −33/7); 7. *Spiroplectammina spectabilis* (BRI +50); 8. *Rashnovammina munda* (BRI −50,5); 9. *Haplophragmoides* cf.*kirki*. (BRI +5); 10. *Saccammina placenta* (BRI −25.5); 11. *Glomospira irregularis* (BRI +35); 12. *Glomospira charoides* (BRI −75.5); 13. *Osangularia* sp. (BRI +15); 14. *Globocassidulina subglobosa* (BRI +15); 15. *Tappanina selmensis* (BRI +15); 16. *Tappanina selmensis* (BRI −9); 17. *Siphogenerinoides brevispinosa* (BRI −11); 18. *Siphogenerinoides brevispinosa* (BRI −365); 19. *Bulimina tuxpamensis* (BRI +150); 20. *Bulimina tuxpamensis* (BRI +150); 21. *Pleurostomella* sp. (BRI +150); 22. *Bolivina* sp. costate (BRI +385); 23. *Nuttallides truempyi* (BRI +150); 24. *Oridorsalis umbonatus* (BRI −135.5); 25. *Aragonia aragonensis* (BRI −105); 26. *Abyssammina poagi* (TAL7B).

Full Screen / Esc
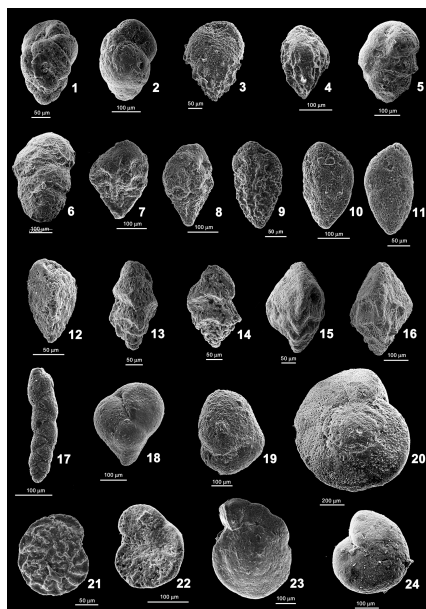
Plate 3. SEM micrographs of the most representative taxa of the upper Paleocene-lower Eocene of Forada section. 1. *Quadratobuliminella pyramidalis* (BRI −75.5); 2. *Buliminella grata* (BRI −591); 3. *Bulimina midwayensis* (BRI +35); 4. *Bulimina alazanensis* (BRI +150); 5, 6. *Bulimina trinitatensis* (BRI −9); 7. *Bolivinoides crenulata* (BRI −9); 8. *Bolivinoides crenulata* (BRI −25.5); 9. *Bolivinoides floridana* (BRI −410); 10 *Bolivina* sp. smooth (BRI −410); 11. *Bolivina* sp. smooth (BRI −410); 12. *Reussella* sp. (BRI −365); 13. *Angulogerina muralis* (BRI −75.5); 14. *Angulogerina muralis* (BRI −75.5); 15. *Angulogerina*? sp. (BRI −9); 16. *Angulogerina*? sp. (BRI −35.5); 17. *Rectobulimina carpentierae* (BRI −466); 18. *Allomorphina trochoides* (BRI −25.5); 19. *Quadrimorphina allomorphinoides* (TAL 7B); 20. *Cibicidoides eocaenus* (BRI −9); 21. *Anomalinoides* sp. 2 (BRI −135); 22. *Cibicides* sp. (BRI −591); 23. *Cibicidoides praemundulus* (BRI +150); 24. *Nonion havanense* (BRI −591).
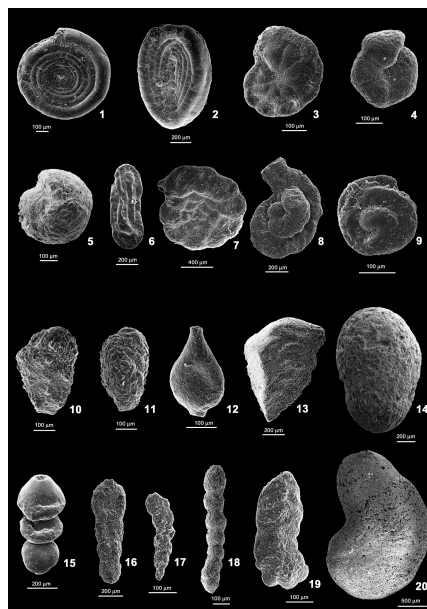
Plate 4. SEM micrographs of some taxa of the upper Paleocene-lower Eocene of Forada section. 1. *Ammodiscus cretaceus* (BRI −29.5); 2. *Ammodiscus peruvianus* (BRI −9); 3. *Haplophragmoides walteri* (BRI −75.5); 4. *Haplophragmoides horridus* (BRI +35); 5. *Recurvoides* sp. (BRI −33/−37); 6. *Glomospira serpens* (BRI −260); 7. *Trochamminoides proteus* (BRI −25.5); 8. *Paratrochamminoides heteromorphus* (BRI +40); 9. *Glomospira* cf. *gordialis* (BRI +35); 10. *Gaudryina* sp. (BRI +15); 11. *Karrerulina coniformis* (BRI −135); 12. *Caudammina ovuloides* (BRI −260); 13. *Gaudryina pyramidata* (BRI −17.5); 14. Big-sized lituolid, apertural view (BRI −9); 15. *Hormosina velascoensis* (BRI −33/37); 16. *Pseudonodosinella troyeri* (BRI −260); 17. ”*Pseudobolivina*” sp. 2 in Galeotti et al. (2004) (BRI +35); 18. *Pseudoclavulina trinitatensis* (BRI +150); 19. *Spiroplectammina spectabilis* (BRI −50.5); 20. Big-sized lituolid, lateral view (BRI −9).